

Aneuploidy can be an evolutionary detour on the path to adaptation

Ilia Kohanovski^{a,b,*}, Martin Pontz^{a,*}, Orna Dahan^c, Yitzhak Pilpel^c, Avihu H.
Yona^d, and Yoav Ram^{a,1}

^aSchool of Zoology, Faculty of Life Sciences, Tel Aviv University, Tel Aviv, Israel

^bSchool of Computer Science, Reichman University, Herzliya, Israel

^cDepartment of Molecular Genetics, Weizmann Institute of Science, Rehovot 76100, Israel

^dInstitute of Biochemistry, Food Science and Nutrition, Robert H. Smith Faculty of Agriculture, Food and Environment, The Hebrew University of Jerusalem, Israel

*These authors contributed equally to this work

¹Corresponding author: yoav@yoavram.com

October 13, 2022

Classifications. Biological Sciences: Evolution, Genetics, Microbiology, Population Biology.

Keywords: whole-chromosome duplication, evolutionary model, adaptive evolution

Abstract

16 Aneuploidy is common in eukaryotes, often leading to decreased growth and fitness. However,
evidence from yeast and fungi, as well as human tumour cells, suggests that specific aneuploidies
18 can be beneficial under stressful conditions and facilitate adaptation. In a prominent example, an
evolutionary experiment with yeast, populations evolving under heat stress had become aneuploid
20 (chromosome III), only to later revert back to euploid after genetic mutations have accumulated. It
has therefore been suggested that aneuploidy serves as a "stepping stone" on the path to adaptation.

22 Here, we test this hypothesis. First, we apply DNA sequencing to show that mutant alleles
common in aneuploid cells are uncommon in the evolved euploid population. Second, we develop
24 an evolutionary model with both aneuploidy and mutation, and fit it to the results of the experiment
using a Bayesian inference framework. We then predict the genotype frequency dynamics during
26 the experiment, demonstrating that the majority of the evolved euploid population likely did not
descend from aneuploid cells, but rather directly from the euploid wild-type population. Our
28 model further predicts that if the experiment was repeated with smaller populations, then a larger
fraction of the evolved population would descend from aneuploid cells.

30 Together, our results suggest that aneuploidy can be an inevitable evolutionary "detour" rather
than a "stepping stone": it can delay, rather than facilitate, the adaptation of the population, and
32 cells that become aneuploid may leave less descendants compared to cells that remain diploid.

Introduction

34 Aneuploidy is an imbalance in the number of chromosomes in the cell: an incorrect karyotype.
Evidence suggests aneuploidy is very common in eukaryotes, e.g. animals^{38,30,2}, and fungi^{33,61,36,50}.
36 Aneuploidy has been implicated in cancer formation, progression, and resistance^{4,40,38,19}. It is also
common in protozoan pathogens of the *Leishmania* genus, a major global health concern²⁸, and
38 contributes to the emergence of drug resistance⁴¹ and virulence²⁹ in fungal pathogens, which are
under-studied³⁷, despite infecting a billion people per year, causing significant morbidity in >150
40 million and death in >1.5 million people per year^{41,37}.

Experiments with human and mouse embryos found that most aneuploidies are lethal. It is also
42 associated with developmental defects and lethality in other multicellular organisms⁴⁴. For example,
aneuploid mouse embryonic cells grow slower than euploid cells⁵⁵. Similarly, in unicellular eukaryotes
44 growing in benign conditions, aneuploidy usually leads to slower growth and decreased overall
fitness^{31,53,33,44,22,56}, in part due to proteotoxic stress caused by increased expression in aneuploid
46 cells^{33,39,60} and hypo-osmotic-like stress⁵⁴.

However, aneuploidy can be beneficial under stressful conditions due to the wide range of phenotypes
48 it can produce, some of which are advantageous^{33,56}. Thus, aneuploidy can lead to rapid adaptation in
unicellular eukaryotes^{14,52,18,35}, as well as to rapid growth of somatic tumour cells^{40,46}. For example,
50 aneuploidy in *Saccharomyces cerevisiae* facilitates adaptation to a variety of stressful conditions
like heat and pH⁵⁸, copper^{7,14}, salt¹⁰, and nutrient limitation^{11,16,1}, with similar results in *Candida*
52 *albicans*⁵⁶. Importantly, aneuploidy can also lead to drug resistance in pathogenic fungi such as
C. albicans^{43,42,13} and *Cryptococcus neoformans*⁴⁷, which cause candidiasis and meningoencephalitis,
54 respectively.

Yona et al.⁵⁸ demonstrated experimentally the importance of aneuploidy in adaptive evolution. They
56 evolved populations of *S. cerevisiae* under strong heat stress. The populations adapted to the heat stress
within 450 generations, and this adaptation was determined to be due a duplication of chromosome III.
58 Later on, after more than 1,500 generations, the populations reverted back to an euploid state, while
remaining adapted to the heat stress. Aneuploidy was therefore suggested to be a *transient adaptive*
60 *solution*, because it can rapidly appear and fixate in the population under stressful conditions, and can
then be rapidly lost when the cost of aneuploidy outweighs its benefit—after the stress is removed,
62 or after "refined" beneficial mutations appear and fixate⁵⁸. Furthermore, it has been suggested that
aneuploidy is an evolutionary "stepping stone" that facilitates future adaptation by genetic mutations,
64 which require more time to evolve^{58,57}.

Here, we test the hypothesis that aneuploidy is a an *evolutionary stepping stone* that facilitates adaptive evolution by genetic mutations. First, we analyze previously unpublished sequencing data from the original experimental populations⁵⁸ to assess if the evolved euploid population is descended from the aneuploid population. Second, we develop an evolutionary genetic model and fit it to the experimental results of Yona et al.⁵⁸ in order to predict the genotype frequency dynamics in the experimental populations, thereby estimating the frequency of evolved euploid cells that descended from aneuploid cells. Our results show that aneuploidy reached high frequencies in the experimental populations, but nevertheless, the majority of cells in the evolved euploid populations likely did not descend from aneuploid cells, but rather directly from wild-type euploid cells. These results suggest that aneuploidy can be an evolutionary detour, rather than a stepping stone, on the path to adaptation.

Results

In the heat-stress experiment of Yona et al.⁵⁸, four populations of *S. cerevisiae* evolved under 39 °C. Aneuploidy fixed in all four experimental repetitions in the first 450 generations. Two of the repetitions, marked *H2* and *H4*, carried no large-scale duplications other than a chromosome III trisomy. These two repetitions continued to evolve under the same conditions, wherein aneuploidy was eliminated by generation 1,700 and 2,350 in *H4* and *H2*, respectively.

Empirical frequencies of mutant alleles. For each of two evolved populations (*H2* and *H4*) we sequenced the ancestral population (generation 0), the aneuploid population (generation 450), and the evolved euploid population (generation 1,700 or 2,350) to estimate the mutant allele frequencies (Tables S1 and S2). Overall, between 100 and 173 mutant alleles were detected with at least a single read in the six populations that were sampled. Disregarding 45 and 40 alleles that were present in the ancestral populations at a frequency >10%, the aneuploid and euploid populations carried a large number of mutant alleles: 82 and 95, respectively, in repetition *H2*, and 60 and 66 in repetition *H4*.

Surprisingly, out of all these mutant alleles, none was present at a frequency >20% in both the aneuploid and the evolved euploid populations. Furthermore, a high mutant allele frequency in the aneuploid population implies a low frequency in the evolved euploid population, and vice-versa (Spearman's correlation coefficient $\rho = -0.64$ and -0.66 in the two experimental repetitions; Figure 1), such that mutant alleles frequent in the aneuploid populations decreased in frequency when aneuploidy was lost. Moreover, for the 18 mutant alleles with high frequency in the aneuploid populations (>20%), the

highest frequencies in the euploid populations were 15.4%, 16%, 16.3% and 19.6% (the rest were below 96 15%). Similarly, for the 48 mutant alleles with high frequency in the evolved euploid populations, the highest frequencies in the aneuploid populations were 2.7%, 7.7%, and 11.1% (the rest were below 98 1%). These results suggest evolved euploid cells are unlikely to descend from aneuploid cells.

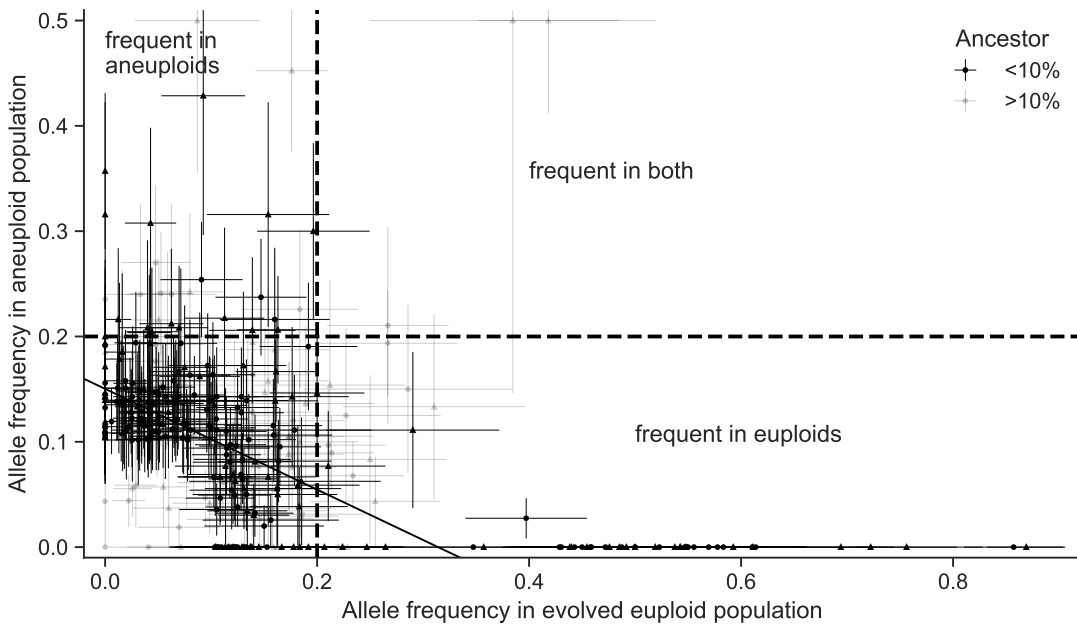


Figure 1: Frequencies of mutant alleles in the experimental populations are negatively correlated. Frequencies of mutant alleles when trisomy was widespread in the population (y-axis) and after it was eliminated (x-axis) in two experimental repetitions (circles for *H2* and triangles for *H4*) from Yona et al.⁵⁸. Mutant alleles with >20% in the aneuploid population were <20% in the euploid population, and vice versa (the upper-right quadrant is empty), suggesting that the majority of evolved euploid cells did not descend from the most common aneuploid genotypes. Alleles with frequency below and above 10% in the ancestral populations are in black and gray, respectively. Solid black line is a linear orthogonal distance regression line (slope=-0.559, intercept=0.164; a regression through alleles that reach at least 20% in one of the populations has slope=-0.645 and intercept=0.297). Dashed vertical and horizontal lines show allele frequencies 20%. Error bars show standard error of the mean accounting for the number of reads.

Evolutionary genetic model. To explore the dynamics during the evolutionary experiments, we 100 developed an evolutionary genetic model, fitted the model to empirical data, and used it to predict the genotype frequency dynamics, or specifically, the fraction of the evolved euploid population descended 102 from aneuploid cells.

The model includes the effects of natural selection, genetic drift, aneuploidy, and mutation, and follows

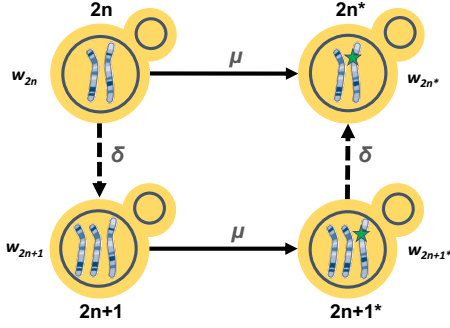


Figure 2: Model Illustration. There are four genotypes in our model: euploid wild-type, $2n$; euploid mutant, $2n^*$; aneuploid wild-type, $2n+1$; and aneuploid mutant, $2n+1^*$. Overall there are two possible trajectories from $2n$ to $2n^*$. Arrows denote transitions between genotypes, with transition rates μ for the beneficial mutation rate and δ for the aneuploidy rate.

104 a population of cells characterized by their genotype: euploid wild-type, $2n$, is the ancestral diploid
 106 genotype; euploid mutant, $2n^*$, has a diploid karyotype and a single beneficial mutation; aneuploid
 108 wild-type, $2n+1$, has an extra chromosome due to a chromosome duplication event; and aneuploid
 110 mutant, $2n+1^*$, has and extra chromosome and a beneficial mutation. Fitness values of the different
 112 genotypes are denoted by w_{2n} , w_{2n^*} , w_{2n+1} , and w_{2n+1^*} , and the rate of mutation and aneuploidy are
 114 denoted by μ and δ . See Figure 2 for an illustration of the model.

116 We fitted this model to the experimental results⁵⁸ – time for fixation ($>95\%$) and for loss ($<5\%$) of
 118 aneuploidy – using approximate Bayesian computation with sequential Monte Carlo (ABC-SMC)⁴⁸,
 thereby inferring the model parameters: rates aneuploidy and mutation and the fitness of all genotypes.
 We then sampled posterior predictions for the genotype frequency dynamics using the estimated
 120 parameter values and compared different versions of the model to test additional hypotheses about the
 evolutionary process.

122 **Estimated rates and fitness effects of aneuploidy and mutation.** We inferred the posterior distribution
 124 of model parameters (Figure 3). We report parameter estimates using the MAP (maximum a
 posteriori) and providing the 50% HDI (highest density interval) in square brackets. See Supplementary
 Material for sensitivity analysis.

126 The estimated beneficial mutation rate is $\mu = 2.965 \cdot 10^{-6}$ [$2.718 \cdot 10^{-7} - 3.589 \cdot 10^{-6}$]. From the
 literature, the mutation rate per base pair is roughly $2 - 3 \cdot 10^{-10}$ (refs.^{62,27}), but it may be higher
 128 under heat stress, as several stresses may cause hypermutation in yeast¹⁷. If we assume a 10-fold
 increase in mutation rate, then the estimated beneficial mutation rate can be explained by a target size
 130 of 1,000 base pairs. Yona et al.⁵⁸ found at least 10 genes on chromosome III with mutations that

led to increased heat tolerance. Assuming that other chromosomes also have a similar number of
126 heat-tolerance genes (i.e., chromosome III is one of the smaller chromosomes¹⁵), and that each gene
has a target size of ten base pairs, we easily get to a target size above 1,600.

128 The estimated aneuploidy rate, $\delta = 1.72 \cdot 10^{-3}$ [$1.47 \cdot 10^{-3} - 2.786 \cdot 10^{-3}$] is higher than in previous
studies: for chromosome III in diploid *S. cerevisiae*, Zhu et al.⁶² estimated $6.7 \cdot 10^{-6}$ chromosome
130 gain events per generation, and Kumaran et al.²⁶ estimate $3.0 - 4.3 \cdot 10^{-5}$ chromosome loss events
per generation (95% confidence interval). However, this difference may be explained by an increased
132 aneuploidy rate during heat stress⁵.

The estimated fitness values are $w_{2n+1} = 1.022$ [1.021 – 1.023], $w_{2n+1^*} = 1.025$ [1.024 – 1.026],
134 $w_{2n^*} = 1.028$ [1.026 – 1.029], all relative to the fitness of $2n$, which is set to $w_{2n} = 1$. Thus, we
can infer that the cost of chromosome III trisomy is $c = w_{2n^*} - w_{2n+1^*} = 0.003$ (or 0.3%) and the
136 benefit of trisomy is $w_{2n+1} - 1 - c = 0.019$ (1.9%), whereas the benefit of the beneficial mutation is
 $w_{2n^*} - 1 = 0.028$ (2.8%).

138 If we allow for transitions (mutation, chromosome loss and gain) to less-fit genotypes (e.g., $2n^*$ to
 $2n+1^*$), then we infer similar but slightly different values, see Supplementary Material.

140 **Model comparison and goodness-of-fit.** Our model fits the data well: in simulations using the MAP
parameter estimates, $2n^*$ fixed in 61% of simulations by generation 1,700 and in 100% of simulations
142 by generation 2,350 (Figure 4B).

However, a model without aneuploidy (where the aneuploidy rate is fixed at zero, $\delta = 0$), fails to
144 explain the experimental observations (Figure 4). The estimated mutation rate without aneuploidy
is $\mu = 7.98 \cdot 10^{-9}$ [$7.906 \cdot 10^{-9} - 8.138 \cdot 10^{-9}$], much lower compared to a model with aneuploidy
146 and suggesting a target size of just 40. The fitness of the mutant is also much lower at $w_{2n^*} =$
 1.013 [1.012 – 1.013]. This is because, without aneuploidy, a high mutation rate or fitness effect will
148 lead to faster appearance and fixation of $2n^*$ than in the experimental observations.

We also checked a model in which aneuploidy occurs but is adaptively neutral compared to the wild-
150 type, that is, $w_{2n+1} = w_{2n}$ and $w_{2n+1^*} = w_{2n^*}$ but $\delta > 0$. This model fits the data better than the model
with no aneuploidy (in which $\delta = 0$), but worse than a model with positive selection for aneuploidy,
152 in which $w_{2n} < w_{2n+1} < w_{2n+1^*} < w_{2n^*}$ (Figure 4).

Model predictions of genotype frequency dynamics. We simulated 50 replicate genotype fre-
154 quency dynamics using the MAP estimate parameters. Figure 5A shows the simulated frequencies of

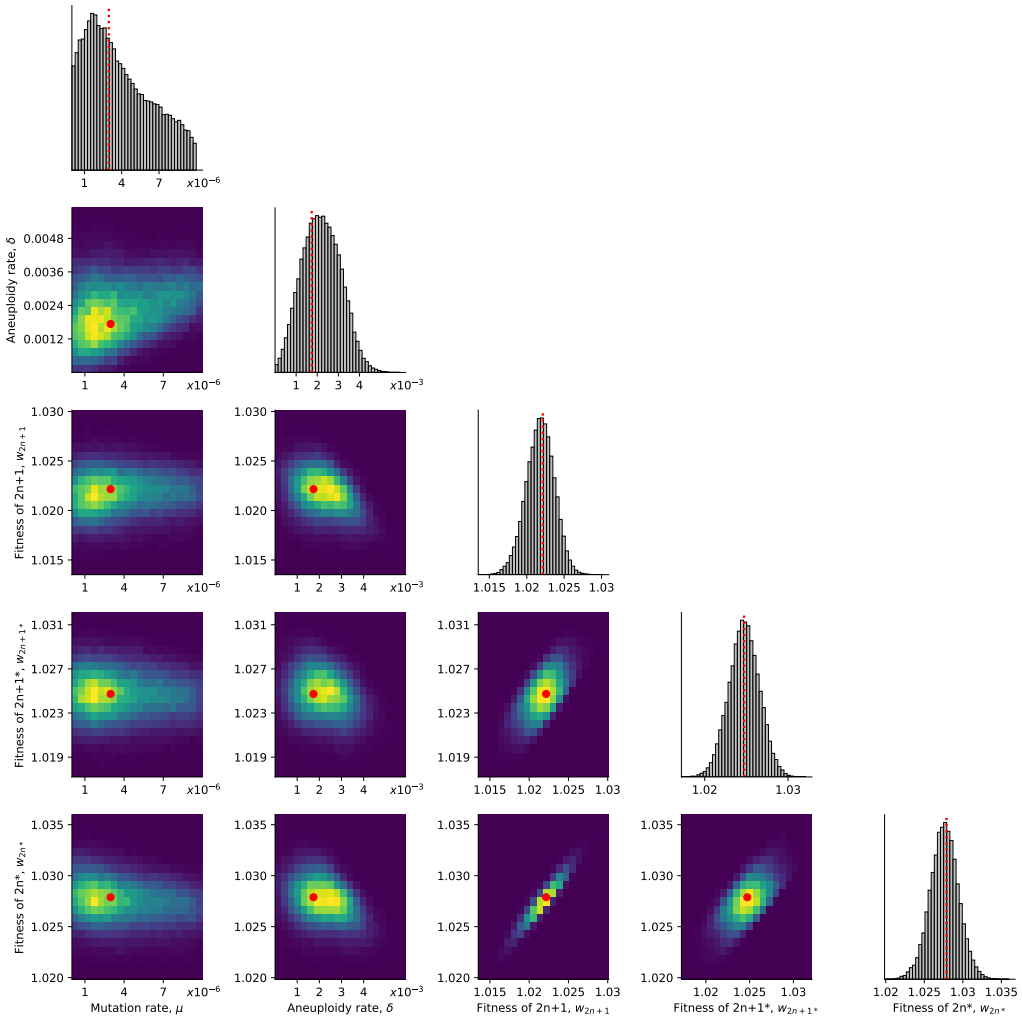


Figure 3: Posterior distribution of model parameters. On the diagonal, the marginal posterior distribution of each model parameter. Below the diagonal, the joint posterior distribution of pairs of model parameters (dark purple and bright yellow for low and high density, respectively). Red markers and orange lines for the joint MAP estimate (which may differ from the marginal MAP, as the marginal distribution integrates over all other parameters).

the four genotypes ($2n$, $2n+1$, $2n+1^*$ and $2n^*$), as well as the frequencies of $2n^*$ cells that arose from
 156 either $2n+1$ cells via a sequences of mutation and chromosome loss events ($2n_A^*$), or directly from
 $2n$ cells via a mutation event ($2n_M^*$). We find that $2n+1^*$ never reaches substantial frequency as it is
 158 quickly replaced by $2n^*$ in a process similar to *stochastic tunneling*^{20,25}.

To test the hypothesis that aneuploidy facilitates adaptation, we estimated F_A , the expected frequency
 160 of $2n^*$ that arose from $2n+1$, computed as the average frequency of such $2n_A^*$ cells at the end of
 simulations using the MAP estimate parameters. Surprisingly, we observe that the majority of $2n^*$
 162 cells are $2n_M^*$, a product of a direct mutation in $2n$ cells, rather than descending from $2n+1$ cells
 $(F_A^{MAP} = 0.106$, average end point of 50 purple lines in Figure 5A). This is despite the fact that the

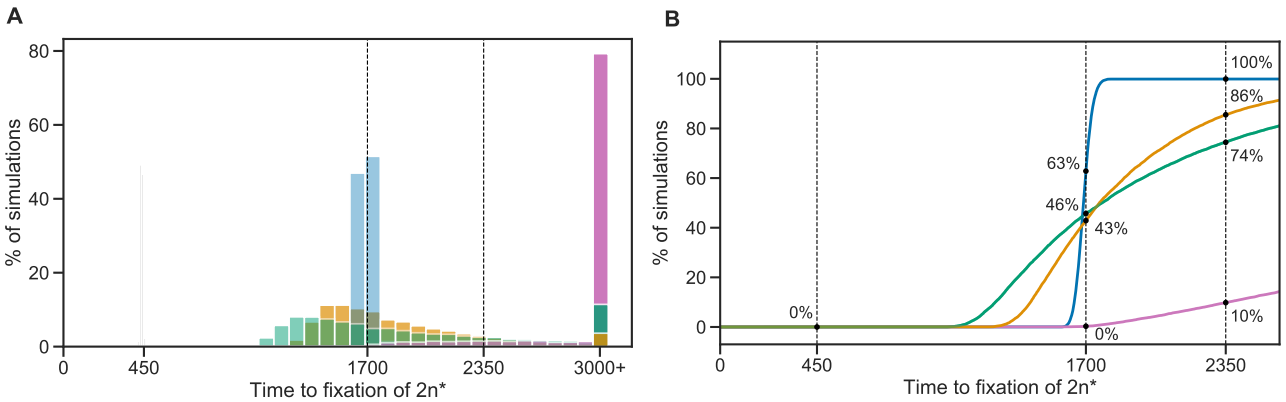


Figure 4: Model fit with and without aneuploidy. The distribution of time to fixation of $2n^*$ (i.e., adaptation time) in 10,000 simulations using MAP parameters of the model with beneficial aneuploidy (blue; $\delta > 0$, $w_{2n} < w_{2n+1} < w_{2n+1^*} < w_{2n^*}$) compared to alternative models: a model with the same parameter values but without aneuploidy (gray, $\delta = 0$, concentrated at $t = 450$); a model fitted to the data assuming no aneuploidy (green, $\delta = 0$); a model fitted to the data assuming neutral aneuploidy (yellow, $\delta > 0$, $w_{2n+1} = w_{2n}$, $w_{2n+1^*} = w_{2n^*}$); and a model with beneficial aneuploidy and an extended prior distribution (pink). In the experiment by Yona et al.⁵⁸, one population lost aneuploidy by generation 1,700 and another by generation 2,350 (dashed lines) but not before generation 450. Thus, the blue distribution has a better fit compared to the other distributions (the gray distribution has a particularly poor fit). The MAP likelihood (eq. (4)) is 0.84, 0.78, 0.67, and 0.14 for the models represented by blue, yellow, green, and pink distributions, respectively. **(A)** Histogram of the time to fixation of $2n^*$. The last bin contains all values equal or greater than 3,000. **(B)** Cumulative distribution of the time to fixation.

164 2 $n+1$ genotype reaches high frequencies in the population (at least 0.98, Figure 5A).

This result is not unique to the MAP parameter estimate. We simulated genotype frequency dynamics
 166 using parameter samples from the posterior distribution, and computed the posterior distribution of F_A
 (Figure 5B). The posterior mode F_A was just 0.147 [0.0154-0.370 95% CI] and only in 489 of 100,000
 168 posterior samples (0.489%) F_A was larger than 0.5 (see Supporting Material for results when transitions
 to less-fit genotypes are allowed, such as $2n^*$ to $2n+1^*$). Thus, if we sample a random cell from the
 170 evolved $2n^*$ population, it is more likely to have descended directly from an euploid cell than from
 an aneuploid cell. The probability of $2n^*$ descending from $2n+1$ (F_A) increases with the aneuploidy
 172 rate, δ , and decreases with both the population size N and the mutation rate, μ (Figure 5C,D). In some
 cases it can also be affected by the fitness parameters (Figure S10).

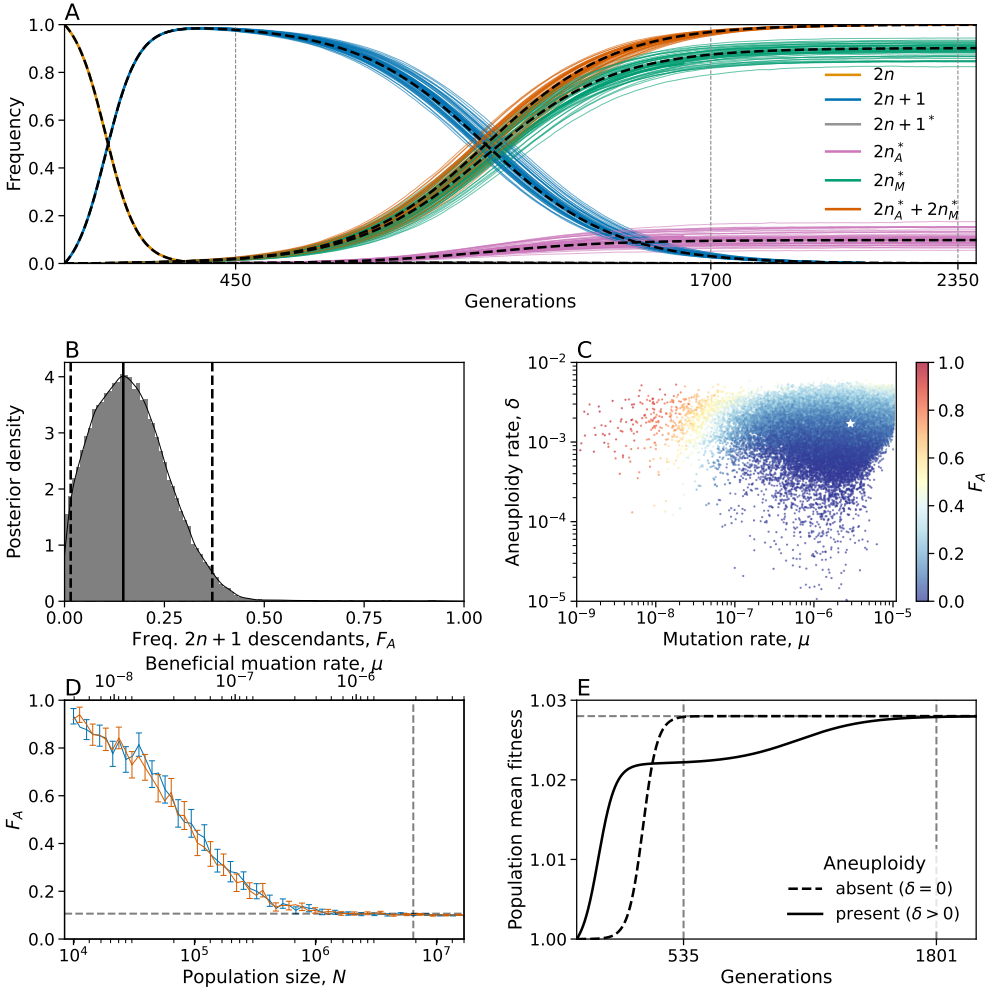


Figure 5: Predicted frequency of aneuploid-descended cells. (A) Posterior predicted genotype frequencies over time, including the source of $2n^*$: $2n_A^*$ arose from $2n + 1$, whereas $2n_M^*$ arose directly from $2n$. Colored curves are 50 simulations using the MAP estimate parameters. Black dashed curves are the expected genotype frequencies without genetic drift (from a deterministic model). See Figure S9 for log-log scale, in which the sequence of events is easier to observe. (B) Posterior distribution of F_A , the expected frequency of $2n^*$ cells descended from $2n+1$ cells, computed as the average frequency at the end of 100 simulations for 100,000 samples from the parameter posterior distribution. Solid and dashed lines show the mode and 95% CI. (C) F_A values (color coded) from panel B, with their corresponding mutation rate μ on x-axis and aneuploidy rate δ on the y-axis. White star shows the MAP estimate. See also Figure S10. (D) F_A as a function of the population size (N , bottom x-axis) and the beneficial mutation rate (μ , top x-axis) in posterior predictions with MAP parameters. Markers show F_A in 250 simulations per population size or mutation rate value. Error bars show mean F_A with 95% CI (bootstrap, $n = 10,000$). Blue and red bars for varying population size and mutation rate, respectively. Vertical dashed line for population size in the experiment, $6.425 \cdot 10^6$, and the MAP mutation rate, $2.965 \cdot 10^{-6}$. Horizontal line for $F_A^{MAP} = 0.106$. (E) Population mean fitness in a model without drift using MAP estimate parameters. Solid lines for mean fitness with aneuploidy ($\delta > 0$), where the population reaches adaptation (mean fitness at 99.99% of maximum value) at generation 1,802. Dashed lines for mean fitness without aneuploidy ($\delta = 0$), where the population adapts much earlier, at generation 535.

174 **Genetic instability in aneuploid cells.** It has been suggested that aneuploidy increases genetic
175 instability^{45,19}. Therefore, we inferred model parameters under the assumption that the mutation rate
176 increases in aneuploid cells by a factor $\tau = 1, 33/32$ (due to an additional chromosome), 2, 5, 10, or
177 100 (due to genetic instability). We found that the posterior distribution was similar for $\tau = 1, 33/32$,
178 2, and 5 (Figure S4). With $\tau = 100$, the estimated mutation rate was about 7-8-fold lower compared
179 to $\tau = 1$ ($\mu = 4.094 \cdot 10^{-7}$ [$6.252 \cdot 10^{-8} - 6.046 \cdot 10^{-7}$]) and the aneuploidy rate was about 2-3-fold
180 lower ($\delta = 0.744 \cdot 10^{-3}$ [$0.506 \cdot 10^{-3} - 1.827 \cdot 10^{-3}$]). With $\tau = 10$, the estimated mutation rate
181 was only slightly lower compared to $\tau = 1$ ($\mu = 1.67 \cdot 10^{-6}$ [$2.836 \cdot 10^{-8} - 2.245 \cdot 10^{-6}$]). WAIC
182 (lower is better, see Methods) is lowest for $\tau = 33/32$ and $\tau = 1$ (Table S3). Therefore, our results do
183 not support an increase in mutation rate in aneuploid cells. This may be because, unless the increase
184 is strong ($\tau \geq 10$), it does not seem to affect our inference; or because chromosome III is one of
185 the smallest chromosomes¹⁵. We also checked the differences in genotype frequency dynamics for
186 different τ values. We observe $\tau = 100$ could be distinguished if accurate data was available for the
187 waiting time until the frequency of $2n$ to decrease below 95% (Figure S5A) or for waiting time for the
188 frequency of $2n+1$ to either reach or go below 95% (Figure S5B).

Discussion

190 In a landmark study on the role of chromosome duplication in adaptive evolution, Yona et al.⁵⁸
191 found that a chromosome III trisomy was acquired by *S. cerevisiae* populations evolving under heat
192 stress, only to be later replaced by euploid mutant cells that carry "refined" solutions to the stress.
193 Additionally, such a replacement also occurred when they initiated evolutionary experiments with a
194 population in which all cells carry a chromosome III trisomy. They hypothesized that the euploid
195 mutant cells evolved by heat-resistance mutations in aneuploid cells followed by reversion of trisomy
196 due to a chromosome loss event.

197 If indeed the evolved euploid population is descended from the aneuploid population, then mutant
198 alleles that were common in the aneuploid populations should also be common in the evolved euploid
199 population. However, we found that this is not the case (Figure 1): mutant allele frequencies in the
200 aneuploid and euploid populations are negatively correlated, such that common alleles in the former
201 are rare in the latter. Furthermore, we developed an evolutionary genetic model of adaptive evolution
202 by aneuploidy and mutation (Figure 2), fitted it to the experimental results of Yona et al.⁵⁸, and
203 used it to predict the genotype frequency dynamics. The model predicted that only about 10-15% of
204 the evolved euploid population descended from aneuploid cells—that is, the majority of the euploid

population are not descended from aneuploid cells, but rather are direct descendants of the ancestral
206 wild-type population (Figure 5).

This happens despite aneuploidy reaching a high frequency in the population (>95%). Conventional
208 wisdom might suggest that once the aneuploid genotype $2n+1$ reaches high frequency, it will have a
better chance at producing "refined" solutions via mutations, and its descendants will come to dominate
210 the population: the frequency of $2n_A^*$ (which arises from $2n+1^*$) will be higher than the frequency of
 $2n_M^*$ (which arises directly from $2n$).

212 So how does $2n_M^*$ prevail? Initially, the supply rates of $2n+1$ and $2n_M^*$ are $N\delta \approx 11,000$ and $N\mu \approx 19$,
respectively (assuming MAP parameter estimates). Therefore, both genotypes are expected to appear
214 immediately at the beginning of the experiment (Figure S9). However, $2n+1$ appears at a much higher
frequency as $\delta \gg \mu$ by 2-3 orders of magnitude. After they first appear, $2n_M^*$ has higher fitness. But
216 as long as the frequency of $2n$ is high, the supply rate of $2n+1$ is higher than that of $2n_M^*$, again due to
 $\delta \gg \mu$. However, supply rates of both genotypes decreases with the frequency of $2n$. Therefore, when
218 the latter decreases, mainly due to the increase in the frequency of $2n+1$, both supply rates diminish.
At this stage, the higher fitness of $2n_M^*$ comes into play and it starts to take over the population,
220 which is mainly composed of $2n+1$. For the aneuploid lineage to compete with the mutant lineage, it
must produce $2n_A^*$ via a mutation followed by chromosome loss. Although this is a stochastic process
222 (due to drift), our results show that the time until $2n_A^*$ reaches a frequency of 0.1% is roughly 450
generations, without much variation (intersection of purple lines and vertical dashed line in Figure S9).
224 However, by that time $2n_M^*$ is already at a roughly 10-fold higher frequency (1.86%), and since both
mutants have the same fitness, their relative frequency remains roughly the same until the end of the
226 experiment.

Predictions for small populations and low mutation rates. We examined the effect of the pop-
228 ulation size, N , and the beneficial mutation rate, μ , on the frequency of $2n+1$ descendants in the
evolved population, F_A . We found that F_A is expected to decrease as the population size or mutation
230 rate increase (Figure 5D), ranging from >90% when the population size is 10,000 or the mutation
rate is $6 \cdot 10^{-9}$, to about 10% when the population size is above 1,000,000 (less than the experimental
232 population size, which was 6,425,000) or the mutation rate is above $2 \cdot 10^{-6}$ (less than the inferred
mutation rate, which is $2.965 \cdot 10^{-6}$). Thus, our model provides a testable prediction: if the experiment
234 was repeated under a lower population size (via stronger daily dilutions or in a smaller volume) or a
lower mutation rate (via a non-mutagenic stress or stress with a smaller target size), then the fraction
236 of the population descending from aneuploid cells would be much higher.

Aneuploidy delays rather than facilitates adaptation. An additional interesting result of our
238 study is that aneuploidy increases, rather than decreases, the adaptation time (Figure 5E). This
happens despite the fact that the mean fitness initially increases faster in the presence of aneuploidy
240 (Figure 5E). This is because once $2n+1$ is common, selection for the mutant strain ($2n+1^*$ or $2n^*$) is
weaker compared to when $2n^*$ competes directly with $2n$.

242 Rate and fitness effect of aneuploidy and mutation. We inferred the rates of aneuploidy and
mutation and their effects on fitness. We estimate that the aneuploidy rate (i.e., number of chromosome
244 gains per generation) is $1.7 \cdot 10^{-3}$, higher than a previous estimate of $6.7 \cdot 10^{-6}$ (ref⁶¹). This may be due
to genetic instability caused by heat stress⁵. In addition, we find no evidence for increased mutation
246 rates in aneuploid cells. Previous empirical studies have suggested that genetic instability (e.g.,
elevated mutation rates) in aneuploid cells is due to stress associated with the aneuploid state^{3,6,59,19}.
248 However, in the experiment of Yona et al.⁵⁸, both the wild-type and the aneuploid were under heat
stress, which may explain why we did not find evidence for an increased mutation rate specifically in
250 aneuploid cells.

Conclusions. Here, we tested the hypothesis that aneuploid cells are an evolutionary "stepping
252 stone", or adaptive intermediate, between wild-type euploid cells and mutant euploid cells. Our
results suggest that, although it seems the population goes from euploid to aneuploid and back, this is
254 not the case at the individual level. We estimate that only about 10-15% of the euploid cells descended
from aneuploid cells, whereas the rest are direct descendants of the wild-type euploid cells. Thus,
256 aneuploidy can delay, rather than accelerate, adaptation, and cells that become aneuploid may
leave less descendants than cells that remain euploid. This surprising result reinforces the importance
258 of models when making interpretations on evolutionary processes, and emphasizes the unintuitive
outcomes of clonal interference during adaptive evolution.

260 Models and Methods

DNA sequencing. Whole-genome sequencing of the ancestral diploid strain ($2n$) was performed
262 on a sample from a single colony of the ancestor. Whole-genome sequencing of the four evolving
populations (H_2 after 450 and 2,350 generations, and H_4 after 450 and 1,700 generations) was
264 performed on a sample from these populations (rather than from single colonies). The liquid sample
from each evolving population was taken from each culture as it grows under the same conditions as

266 the lab evolution experiments (YPD at 39 °C). DNA was purified from the collected cells for each
 267 population and downstream deep sequencing was performed according to the Illumina protocol for
 268 amplicon sequencing.

Evolutionary genetic model. We model the evolution of a population of cells using a Wright-Fisher
 270 model³², assuming a constant effective population size N , non-overlapping generations, and including
 271 the effects of natural selection, genetic drift, aneuploidy, and mutation. We focus on beneficial genetic
 272 modifications, neglecting the effects of deleterious and neutral mutations or karyotypic changes. The
 273 model allows for a single aneuploid karyotype (e.g., chromosome III duplication) and a single mutation
 274 to accumulate in the genotype. Thus, the model follows four genotypes (Figure 2): euploid wild-type,
 275 2n, the initial genotype; euploid mutant, 2n*, with the standard karyotype and a single beneficial muta-
 276 tion; aneuploid wild-type, 2n+1, with an extra chromosome, i.e., following chromosome duplication;
 277 and aneuploid mutant, 2n+1*, with an extra chromosome and a beneficial mutation.
 278 Transitions between the genotypes occur as follows (Figure 2): Beneficial mutations from 2n to 2n*
 279 and from 2n+1 to 2n+1* occur with probability μ , the mutation rate. We neglect back-mutations (i.e.,
 280 from 2n* to 2n and from 2n+1* to 2n+1). Aneuploidy is formed by chromosome mis-segregation,
 281 so that cells transition from 2n to 2n+1 and from 2n+1* to 2n* with probability δ , the aneuploidy
 282 rate. That is, we assume chromosomes are gained and lost at the same rate, and we neglect events that
 283 form a less-fit genotype (i.e., 2n+1 to 2n and 2n* to 2n+1*).

284 In the experiment by Yona et al.⁵⁸, the population was grown every day from $1.6 \cdot 10^6$ cells until
 285 reaching stationary phase and then diluted 1:120. Thus, we set the population size to $N = 6.425 \cdot 10^6$,
 286 the harmonic mean of $\{2^k \cdot 1.6 \cdot 10^6\}_{k=0}^7$ ⁹. The initial population has N cells with genotype 2n. The
 287 effect of natural selection on the frequency f_i of genotype $i = 2n, 2n + 1, 2n + 1^*$, or $2n^*$ is given
 288 by

$$f_i^s = \frac{f_i w_i}{\bar{w}}, \quad (1)$$

290 where w_i is the fitness of genotype i and $\bar{w} = \sum_j f_j w_j$ is the population mean fitness. The effect of
 291 mutation and aneuploidy on genotype frequencies is given by

$$\begin{aligned} f_{2n}^m &= (1 - \delta - \mu)f_{2n}^s, \\ f_{2n+1}^m &= \delta f_{2n}^s + (1 - \mu)f_{2n+1}^s, \\ f_{2n+1^*}^m &= \mu f_{2n+1}^s + (1 - \delta)f_{2n+1^*}^s, \\ f_{2n^*}^m &= \mu f_{2n}^s + \delta f_{2n+1}^s + f_{2n^*}^s. \end{aligned} \quad (2)$$

Finally, random genetic drift is modeled using a multinomial distribution³²,

$$294 \quad \mathbf{f}' \sim \frac{1}{N} \cdot \text{Mult}(N, \mathbf{f}^m), \quad (3)$$

where $\mathbf{f}^m = (f_{2n}^m, f_{2n+1}^m, f_{2n+1^*}^m, f_{2n^*}^m)$ are the frequencies of the genotypes after mutation and
296 aneuploidy, \mathbf{f}' are the genotype frequencies in the next generation, and $\text{Mult}(N, \mathbf{f})$ is a multinomial
distribution parameterized by the population size N and the genotype frequencies \mathbf{f} . Overall, the change
298 in genotype frequencies from one generation to the next is given by the transformation $f_i \rightarrow f'_i$.

Empirical data for model inference. We use the results of evolutionary experiments reported by
300 Yona et al.⁵⁸. In their heat-stress experiment, four populations of *S. cerevisiae* evolved under 39 °C.
Aneuploidy fixed in all four population in the first 450 generations. Hereafter, fixation or elimination
302 of a genotype *by generation t* means that more than 95% or less than 5% of the population carry the
genotype at generation t , and possibly earlier. From re-analysis of data not published in the original
304 paper, aneuploidy did not fix before at least 200 generations elapsed. The experiment continued with
two populations, in which aneuploidy was eliminated by generation 1,700 and 2,350 while still under
306 the same conditions of elevated heat (39 °C).

Likelihood function. Because our model, just like the Wright-Fisher model, is non-linear and
308 stochastic, computing the distribution of fixation time $T(g)$ of genotype g for use in the likelihood
function is intractable (it is even hard to use a diffusion-equation approximation due to the model having
310 multiple genotypes, rather than just two). We overcome this problem by approximating the likelihood
using simulations. We simulate 1,000 experiments per parameter vector $\theta = (\mu, \delta, s, b, c)$, resulting in
312 a set of simulated observations $\tilde{\mathbf{X}} = \{\tilde{X}_i\}_{i=1}^{1000}$. We then compute the approximate likelihood,

$$\begin{aligned} \mathcal{L}(\theta) = P^4(200 \leq T(2n + 1) \leq 450) \cdot & \left[1 - \right. \\ & P_{\tilde{\mathbf{X}}}^4(\{T(2n^*) < 1700\} \mid 200 \leq T(2n + 1) \leq 450) - \\ & P_{\tilde{\mathbf{X}}}^4(\{1700 < T(2n^*) < 2350\} \mid 200 \leq T(2n + 1) \leq 450) + \\ & \left. P_{\tilde{\mathbf{X}}}^4(\{T(2n^*) < 1700\} \wedge \{1700 < T(2n^*) < 2350\} \mid 200 \leq T(2n + 1) \leq 450) \right], \end{aligned} \quad (4)$$

314 where $\{ \dots \}$ is the "logical not" operator, $P^4(\dots)$ is the 4th power of $P(\dots)$, and all probabilities
 $P_{\tilde{\mathbf{X}}}(\dots)$ are approximated from the results of the simulations $\tilde{\mathbf{X}}$. For example, $P_{\tilde{\mathbf{X}}}(\{T(2n^*) < 1700\} \mid$
316 $200 \leq T(2n + 1) \leq 450)$ is approximated by taking simulations in which $2n+1$ fixed before generation
450 but not before generation 200, and computing the fraction of such simulations in which $2n^*$ did
318 not fix by generation 1,700, and hence aneuploidy did not extinct before generation 1,700. Figure S1

compares results with less and more simulated experiments, demonstrating that 1,000 simulations are
 320 likely sufficient.

For a model without aneuploidy (that is, when the aneuploidy rate is fixed at zero, $\delta = 0$), we disregard
 322 the increased expression in chromosome III and the growth advantage measured in generation 450, and
 focus on the growth advantage measured in later generations, presumably due to a beneficial mutation.
 324

Therefore, the likelihood is approximated by

$$\begin{aligned} \mathcal{L}_!(\theta) = & 1 - P_{\tilde{\mathbf{X}}}^4(\{T(2n^*) < 1700\}) - \\ & P_{\tilde{\mathbf{X}}}^4(\{1700 < T(2n^*) < 2350\}) + \\ & P_{\tilde{\mathbf{X}}}^4(\{T(2n^*) < 1700\} \wedge \{1700 < T(2n^*) < 2350\}) . \end{aligned} \quad (5)$$

326 **Parameter inference.** To infer model parameters, we use approximate Bayesian computation with
 a sequential Monte-Carlo scheme, or ABC-SMC⁴⁸, implemented in the pyABC Python package²⁴
 328 [pyabc.readthedocs.io](#). This approach uses numerical stochastic simulations of the model to infer
 a posterior distribution over the model parameters. It is a method of likelihood-free, simulation-
 330 based inference⁸, that is, for estimating a posterior distribution when a likelihood function cannot be
 directly computed. It is therefore suitable in our case, in which the likelihood function can only be
 332 approximated from simulations, and cannot be directly computed.

The ABC-SMC algorithm employs sequential importance sampling over multiple iterations^{51,23,49}. In
 334 iteration t of the algorithm, a set of parameter vectors, $\{\theta_{i,t}\}_{i=1}^{n_t}$, also called *particles*, are constructed
 in the following way. A proposal particle, θ^* , is sampled from a proposal distribution, and is either
 336 accepted or rejected, until n_t particles are accepted. The number of particles, n_t , is adapted at every
 iteration t using the adaptive population strategy²⁴ [pyabc.readthedocs.io](#). For $t = 0$, the proposal
 338 particle is sampled from the prior distribution, $p(\theta)$. For $t > 0$, the proposal particle is sampled from
 the particles accepted in the previous iteration, $\{\theta_{i,t-1}\}_{i=1}^{n_{t-1}}$, each with a probability relative to its weight
 340 $W_{t-1}(\theta_{i,t-1})$ (see below). The proposal particle is then perturbed using a kernel perturbation kernel,
 $K_t(\theta^* | \theta)$ where θ is the sample from the previous iteration. Then, a set of synthetic observations
 342 $\tilde{\mathbf{X}}^*$ is simulated, and the proposal particle θ^* is accepted if its approximate likelihood (eq. (4)) is high
 enough, $\mathcal{L}(\theta^*) > 1 - \epsilon_t$ (or more commonly, if $1 - \mathcal{L}(\theta^*) < \epsilon_t$), where $\epsilon_t > 0$ is the *acceptance*
 344 *threshold*, as higher values of ϵ_t allow more particles to be accepted. The acceptance threshold ϵ_t
 is chosen as the median of the $1 - \mathcal{L}(\theta)$ of the particles accepted in the previous iteration, $t - 1$,
 346 and $\epsilon_0 = 0.01$. For each accepted particle $\theta_{i,t}$ a weight $W_t(\theta_{i,t})$ is assigned: for $t = 0$, $W_0(\theta_{i,0}) = 1$,
 and for $t > 0$, $W_t(\theta_{i,t}) = p(\theta_{i,t}) / \sum_{i=1}^{n_{t-1}} W_{t-1}(\theta_{i,t-1}) K_t(\theta_{i,t}, \theta_{i,t-1})$, where $p(\theta)$ is the prior density of θ
 348 and $K_t(\theta' | \theta)$ is the probability of a perturbation from θ to θ' . $K_t(\theta' | \theta)$ is a multivariate normal

distribution, fitted at iteration t to the particles from the previous iteration, $\{\theta_{i,t-1}\}_{i=1}^{n_{t-1}}$, and their
350 weights, $\{W(\theta_{i,t-1})\}_{i=1}^{n_{t-1}}$.

Acceptance is determined according to the approximate likelihood (eq. (4)), which has a maximum
352 value of $\mathcal{L}_{max} = 0.875$ (giving a minimal value of $\epsilon_{min} = 0.125$). We terminated the inference
iterations when the change in ϵ value from one iteration to the next was small. With our standard prior
354 and model, we reached $\epsilon = 0.13$ (or $\mathcal{L} = 0.87$) after six iterations, with $n_6 = 982$ accepted parameter
vectors and effective sample size ESS=651 (Figure S2). Running the inference algorithm with different
356 initialization seeds and less or more simulations for approximating the likelihood produced similar
posterior distributions (Figure S1).

358 After producing a set of weighted particles from the the posterior distribution using the above ABC-
SMC algorithm, we approximate the posterior using kernel density estimation (KDE) with Gaussian
360 kernels. We truncate the estimated posterior to avoid positive posterior density for values with zero
prior density. The MAP (maximum a posteriori) estimate is computed as the the maximum of the
362 estimated joint posterior density. We then draw 5,000,000 samples from the posterior distribution
to compute the HDI (highest density interval) and draw 50,000 samples to visualize the posterior
364 distribution with histograms.

Model comparison. We examine several versions of our evolutionary models, e.g. without aneu-
366 ploidy or with increased mutation rate in aneuploid cells, as well as several different prior distributions
(see below). To compare these, we plot posterior predictions: for each model we execute 10,000
368 simulations using the MAP parameter estimates and plot the distributions of time to fixation of $2n^*$,
one of key properties of the model likelihood. These plots visualize the fit of each model to the
370 data. Also, for similar models we plot the marginal and joint posterior distributions of the parameters;
if these are similar, we consider the models interchangeable. We validate this by comparing HDI
372 (highest density interval) of posterior distributions.

Where posterior plots are very similar and the number of parameters is the same, we use WAIC, or
374 the widely applicable information criterion ¹², defined as

$$WAIC(\theta) = -2 \log \mathbb{E}[\mathcal{L}(\theta)] + 2\mathbb{V}[\log \mathcal{L}(\theta)] \quad (6)$$

376 where θ is a parameter vector, and $\mathbb{E}[\cdot]$ and $\mathbb{V}[\cdot]$ are the expectation and variance taken over the
posterior distribution, which in practice are approximated using 50,000 samples from the posterior
378 KDE. We validated that upon resampling WAIC values do not significantly change and that differences

in WAIC between models are preserved. WAIC values are scaled as a deviance measure: lower values

380 imply higher predictive accuracy²¹.

Prior distributions. We used informative prior distributions for $w_{2n+1} = 1 - c + b$, $w_{2n+1*} =$
382 $(1+s)(1-c)+b$ and $w_{2n*} = 1+s$, which we estimated from growth curves data from mono-culture growth
experiments previously reported by Yona et al.⁵⁸, Figs. 3C, 4A, and S2. We used Curveball, a method
384 for predicting results of competition experiments from growth curve data³⁴ curveball.yoavram.com.

Briefly, Curveball takes growth curves of two strains growing separately in mono-culture and predicts
386 how they would grow in a mixed culture, that is, it predicts the results of a competition assay. From these
predictions, relative fitness values can be computed. Because Curveball uses a maximum-likelihood
388 approach to estimate model parameters, we were able to estimate a distribution of relative fitness
values to be used as a prior distribution by sampling 10,000 samples from a truncated multivariate
390 normal distribution defined by the maximum-likelihood covariance matrix (Figure S3).

We used growth curves of $2n$ and $2n+1$ in 39 °C to estimate an informative prior distribution for
392 w_{2n+1} (Figure S3-D, assuming $w_{2n} = 1$). In this prior distribution, we used the same prior for w_{2n+1*}
and w_{2n*} . To increase computational efficiency, we also assumed $w_{2n*} > w_{2n+1*} > w_{2n+1} > w_{2n}$;
394 running the inference without this assumption produced similar results. See *supporting material* for
an extended informative prior distribution that uses growth curves of $2n*$ and $2n+1$ growing in 39 °C;
396 this prior distribution proved to be less useful.

As a control, we tested an uninformative uniform prior with $U(1, 6)$, for (i) all w_{2n+1} , w_{2n+1*} , w_{2n*} , or
398 (ii) only for w_{2n+1*} , w_{2n*} , using the above informative prior for w_{2n+1} . In these cases the inference
algorithm failed to converge.

400 For the mutation rate, μ , and aneuploidy rate, δ , we used uninformative uniform priors, $\mu \sim$
 $U(10^{-9}, 10^{-5})$ and $\delta \sim U(10^{-6}, 10^{-2})$. A wider mutation rate prior, $\mu \sim U(10^{-9}, 10^{-3})$, produced
402 similar results.

Acknowledgements

404 We thank Lilach Hadany, Judith Berman, David Gresham, Shay Covo, Martin Kupiec, Uri Obolski, Daniel
Weissman, and Tal Simon for discussions and comments. This work was supported in part by the Israel Science
406 Foundation (ISF, YR 552/19), the US–Israel Binational Science Foundation (BSF, YR 2021276) Minerva
Stiftung center for Lab Evolution (YR), Minerva Stiftung short-term research grant (MP).

408 **References**

- [1] Avecilla, G., Chuong, J. N., Li, F., Sherlock, G., Gresham, D. and Ram, Y. 2022, ‘Neural networks enable efficient and accurate simulation-based inference of evolutionary parameters from adaptation dynamics’, *PLOS Biology* **20**(5), e3001633.
- [2] Bakhoum, S. F. and Landau, D. A. 2017, ‘Chromosomal instability as a driver of tumor heterogeneity and evolution’, *Cold Spring Harb. Perspect. Med.* **7**(6), 1–14.
- [3] Bouchonville, K., Forche, A., Tang, K. E. S., Semple, C. a. M. and Berman, J. 2009, ‘Aneuploid chromosomes are highly unstable during dna transformation of *Candida albicans*.’, *Eukaryot. Cell* **8**(10), 1554–66.
- [4] Boveri, T. 2008, ‘Concerning the origin of malignant tumours’, *J. Cell Sci.* **121**(Supplement 1), 1–84.
- [5] Chen, G., Bradford, W. D., Seidel, C. W. and Li, R. 2012, ‘Hsp90 stress potentiates rapid cellular adaptation through induction of aneuploidy.’, *Nature* **482**(7384), 246–50.
- [6] Chen, G., Rubinstein, B. and Li, R. 2012, ‘Whole chromosome aneuploidy: Big mutations drive adaptation by phenotypic leap’, *BioEssays* **34**(10), 893–900.
- [7] Covo, S., Puccia, C. M., Argueso, J. L., Gordenin, D. A. and Resnick, M. A. 2014, ‘The sister chromatid cohesion pathway suppresses multiple chromosome gain and chromosome amplification.’, *Genetics* **196**(2), 373–384.
- [8] Cranmer, K., Brehmer, J. and Louppe, G. 2020, ‘The frontier of simulation-based inference’, *Proceedings of the National Academy of Sciences* p. 201912789.
- [9] Crow, J. F. and Kimura, M. 1970, *An introduction to population genetics theory*, Burgess Pub. Co., Minneapolis.
- [10] Dhar, R. and Sägesser, R and Weikert, C and Yuan, J and Wagner, Andreas, doi = 10.1111/j.1420-9101.2011.02249.x, i . . j . . J. m . . m. n . . p . . p . . t . . A. v . . y . . n.d..
- [11] Dunham, M. J., Badrane, H., Ferea, T., Adams, J., Brown, P. O., Rosenzweig, F. and Botstein, D. 2002, ‘Characteristic genome rearrangements in experimental evolution of *Saccharomyces cerevisiae*’, *Proc. Natl. Acad. Sci.* **99**(25), 16144–16149.
- [12] Gelman, A., Carlin, J. B., Stern, H. S., Dunson, D. B., Vehtari, A. and Rubin, D. B. 2013, *Bayesian Data Analysis, Third Edition*, Chapman & Hall/CRC Texts in Statistical Science, Taylor & Francis.

- 438 [13] Gerstein, A. C. and Berman, J. 2018, ‘Diversity of acquired adaptation to fluconazole is influenced
by genetic background and ancestral fitness in *Candida albicans*’, *bioRxiv* p. 360347.
- 440 [14] Gerstein, A. C., Ono, J., Lo, D. S., Campbell, M. L., Kuzmin, A. and Otto, S. P. 2015, ‘Too
much of a good thing: the unique and repeated paths toward copper adaptation.’, *Genetics*
442 **199**(2), 555–71.
- [15] Gilchrist, C. and Stelkens, R. 2019, ‘Aneuploidy in yeast: Segregation error or adaptation
444 mechanism?’, *Yeast* **36**(9), 525–539.
- 446 [16] Gresham, D., Desai, M. M., Tucker, C. M., Jenq, H. T., Pai, D. A., Ward, A., DeSevo, C. G.,
Botstein, D. and Dunham, M. J. 2008, ‘The repertoire and dynamics of evolutionary adaptations
to controlled nutrient-limited environments in yeast’, *PLoS Genet.* **4**(12).
- 448 [17] Heidenreich, E. 2007, ‘Adaptive Mutation in *< i>Saccharomyces cerevisiae</i>*’, *Crit. Rev.
Biochem. Mol. Biol.* **42**(4), 285–311.
- 450 [18] Hong, J. and Gresham, D. 2014, ‘Molecular specificity, convergence and constraint shape adap-
tive evolution in nutrient-poor environments’, *PLoS Genet.* **10**(1).
- 452 [19] Ippolito, M. R., Martis, V., Martin, S., Tijhuis, A. E., Hong, C., Wardenaar, R., Dumont,
M., Zerbib, J., Spierings, D. C., Fachinetti, D., Ben-David, U., Foijer, F. and Santaguida, S.
454 2021, ‘Gene copy-number changes and chromosomal instability induced by aneuploidy confer
resistance to chemotherapy’, *Dev. Cell* **56**(17), 2440–2454.e6.
- 456 [20] Iwasa, Y., Michor, F. and Nowak, M. A. 2004, ‘Stochastic tunnels in evolutionary dynamics’,
Genetics **166**(3), 1571–1579.
- 458 [21] Kass, R. E. and Raftery, A. E. 1995, ‘Bayes factors’, *J. Am. Stat. Assoc.* **90**(430), 773.
- [22] Kasuga, T., Bui, M., Bernhardt, E., Swiecki, T., Aram, K., Cano, L. M., Webber, J., Brasier,
460 C., Press, C. and Grünwald, Niklaus J. and Rizzo, David M. and Garbelotto, Matteo, doi
= 10.1186/s12864-016-2717-z, i...i...j..B. n...p...p...p...p..B. t..H. v...y...n.d..
- 462 [23] Klinger, E. and Hasenauer, J. 2017, A scheme for adaptive selection of population sizes in
approximate bayesian computation - sequential monte carlo, in J. Feret and H. Koepll, eds,
464 ‘Computational Methods in Systems Biology’, Vol. 10545, Springer International Publishing,
pp. 128–144. Series Title: Lecture Notes in Computer Science.
- 466 [24] Klinger, E., Rickert, D. and Hasenauer, J. 2018, ‘pyabc: distributed, likelihood-free inference’,
Bioinformatics (May), 1–3.

- 468 [25] Komarova, N. L., Sengupta, A. and Nowak, M. A. 2003, ‘Mutation-selection networks of cancer
initiation: Tumor suppressor genes and chromosomal instability’, *J. Theor. Biol.* **223**(4), 433–
470 450.
- 472 [26] Kumaran, R., Yang, S.-Y. and Leu, J.-Y. n.d., ‘Characterization of chromosome stability in
diploid, polyploid and hybrid yeast cells’, **8**(7), e68094.
- 474 [27] Lynch, M., Sung, W., Morris, K., Coffey, N., Landry, C. R., Dopman, E. B., Dickinson, W. J.,
Okamoto, K., Kulkarni, S., Hartl, D. L. and Thomas, W. K. 2008, ‘A genome-wide view of the
spectrum of spontaneous mutations in yeast’, *Proceedings of the National Academy of Sciences*
476 **105**(27), 9272–9277.
- 478 [28] Mannaert, A., Downing, T., Imamura, H. and Dujardin, J. C. 2012, ‘Adaptive mechanisms in
pathogens: Universal aneuploidy in *Leishmania*’, *Trends Parasitol.* **28**(9), 370–376.
- 480 [29] Möller, M., Habig, M., Freitag, M. and Stukenbrock, E. H. 2018, ‘Extraordinary genome
instability and widespread chromosome rearrangements during vegetative growth’, *Genetics*
210(2), 517–529.
- 482 [30] Naylor, R. M. and van Deursen, J. M. 2016, ‘Aneuploidy in cancer and aging’, *Annu. Rev. Genet.*
50(1), 45–66.
- 484 [31] Niwa, O., Tange, Y. and Kurabayashi, A. 2006, ‘Growth arrest and chromosome instability in
aneuploid yeast’, *Yeast* **23**(13), 937–950.
- 486 [32] Otto, S. P. and Day, T. 2007, *A biologist’s guide to mathematical modeling in ecology and
evolution*, Princeton University Press.
- 488 [33] Pavelka, N., Rancati, G., Zhu, J., Bradford, W. D., Saraf, A., Florens, L., Sanderson, B. W., Hat-
tem, G. L. and Li, R. 2010, ‘Aneuploidy confers quantitative proteome changes and phenotypic
490 variation in budding yeast.’, *Nature* **468**(7321), 321–5.
- 492 [34] Ram, Y., Dellus-Gur, E., Bibi, M., Karkare, K., Obolski, U., Feldman, M. W., Cooper, T. F.,
Berman, J. and Hadany, L. 2019, ‘Predicting microbial growth in a mixed culture from growth
curve data’, *Proceedings of the National Academy of Sciences* **116**(29), 14698–14707.
- 494 [35] Rancati, G., Pavelka, N., Fleharty, B., Noll, A., Trimble, R., Walton, K., Perera, A., Staehling-
Hampton, K., Seidel, C. W. and Li, R. 2008, ‘Aneuploidy underlies rapid adaptive evolution of
496 yeast cells deprived of a conserved cytokinesis motor’, *Cell* **135**(5), 879–893.

- [36] Robbins, N., Caplan, T. and Cowen, L. E. 2017, ‘Molecular evolution of antifungal drug resistance’, *Annu. Rev. Microbiol.* **71**(1), 753–775.
498
- [37] Rodrigues, M. L. and Albuquerque, P. C. 2018, ‘Searching for a change: The need for increased support for public health and research on fungal diseases’, *PLoS Negl. Trop. Dis.* **12**(6), 1–5.
500
- [38] Santaguida, S. and Amon, A. 2015, ‘Short- and long-term effects of chromosome mis-segregation and aneuploidy’, *Nat. Rev. Mol. Cell Biol.* **16**(8), 473–485.
502
- [39] Santaguida, S., Vasile, E., White, E. and Amon, A. 2015, ‘Aneuploidy-induced cellular stresses limit autophagic degradation’, *Genes Dev.* **29**(19), 2010–2021.
504
- [40] Schvartzman, J. M., Sotillo, R. and Benezra, R. 2010, ‘Mitotic chromosomal instability and cancer: Mouse modelling of the human disease’, *Nat. Rev. Cancer* **10**(2), 102–115.
506
- [41] Selmecki, A. M., Dulmage, K., Cowen, L. E., Anderson, J. B. and Berman, J. 2009, ‘Acquisition of aneuploidy provides increased fitness during the evolution of antifungal drug resistance’, *PLoS Genet.* **5**(10), e1000705.
508
- [42] Selmecki, A. M., Forche, A. and Berman, J. 2010, ‘Genomic plasticity of the human fungal pathogen *Candida albicans*’, *Eukaryot. Cell* **9**(7), 991–1008.
510
- [43] Selmecki, A. M., Gerami-Nejad, M., Paulson, C., Forche, A. and Berman, J. 2008, ‘An isochromosome confers drug resistance in vivo by amplification of two genes, erg11 and tac1’, *Mol. Microbiol.* **68**(3), 624–641.
512
- [44] Sheltzer, J. M. and Amon, A. 2011, ‘The aneuploidy paradox: Costs and benefits of an incorrect karyotype’, *Trends Genet.* **27**(11), 446–453.
516
- [45] Sheltzer, J. M., Blank, H. M., Pfau, S. J., Tange, Y., George, B. M., Humpton, T. J., Brito, I. L., Hiraoka, Y., Niwa, O. and Amon, A. 2011, ‘Aneuploidy drives genomic instability in yeast’, *Science* **333**(6045), 1026–1030.
518
- [46] Sheltzer, J. M., Ko, J. H., Replogle, J. M., Habibe Burgos, N. C., Chung, E. S., Meehl, C. M., Sayles, N. M., Passerini, V., Storchova, Z. and Amon, A. 2017, ‘Single-chromosome gains commonly function as tumor suppressors’, *Cancer Cell* **31**(2), 240–255.
520
- [47] Sionov, E., Lee, H., Chang, Y. C. and Kwon-Chung, K. J. 2010, ‘*Cryptococcus neoformans* overcomes stress of azole drugs by formation of disomy in specific multiple chromosomes’, *PLoS Pathog.* **6**(4), e1000848.
524

- 526 [48] Sisson, S. A., Fan, Y. and Tanaka, M. M. 2007, ‘Sequential monte carlo without likelihoods’,
Proceedings of the National Academy of Sciences **104**(6), 1760–1765.
- 528 [49] Syga, S., David-Rus, D. and Schälte, Yannik and Hatzikirou, Haralampos and Deutsch, Andreas,
doi = 10.1038/s41598-021-01407-y, j. . S. n. . p. . t. . I. v. . y. . n.d..
- 530 [50] Todd, R. T., Forche, A. and Selmecki, A. M. 2017, ‘Ploidy variation in fungi: Polyploidy,
aneuploidy, and genome evolution’, *Microbiol. Spectr.* **5**(4), 1–20.
- 532 [51] Toni, T., Welch, D., Strelkowa, N., Ipsen, A. and Stumpf, M. P. 2009, ‘Approximate bayesian
computation scheme for parameter inference and model selection in dynamical systems’, *J. R.
Soc. Interface* **6**(31), 187–202.
- 534 [52] Torres, E. M., Dephoure, N., Panneerselvam, A., Tucker, C. M., Whittaker, C. A., Gygi, S. P.,
Dunham, M. J. and Amon, A. 2010, ‘Identification of aneuploidy-tolerating mutations’, *Cell*
143(1), 71–83.
- 538 [53] Torres, E. M., Sokolsky, T., Tucker, C. M., Chan, L. Y., Boselli, M., Dunham, M. J. and Amon,
A. 2007, ‘Effects of aneuploidy on cellular physiology and cell division in haploid yeast’, *Science*
540 (80-.). **317**(5840), 916–924.
- 542 [54] Tsai, H. J., Nelliat, A. R., Choudhury, M. I., Kucharavy, A., Bradford, W. D., Cook, M. E., Kim,
J., Mair, D. B., Sun, S. X., Schatz, M. C. and Li, R. 2019, ‘Hypo-osmotic-like stress underlies
general cellular defects of aneuploidy’, *Nature* .
- 544 [55] Williams, B. R., Prabhu, V. R., Hunter, K. E., Glazier, C. M., Whittaker, C. a., Housman,
D. E. and Amon, A. 2008, ‘Aneuploidy affects proliferation and spontaneous immortalization in
546 mammalian cells’, *Science* **322**(5902), 703–709.
- 548 [56] Yang, F., Todd, R. T., Selmecki, A., Jiang, Y. Y., Cao, Y. B. and Berman, J. 2021, ‘The fitness
costs and benefits of trisomy of each *Candida albicans* chromosome’, *Genetics* **218**(2), 1–7.
- 550 [57] Yona, A. H., Frumkin, I. and Pilpel, Y. 2015, ‘A relay race on the evolutionary adaptation
spectrum’, *Cell* **163**(3), 549–559.
- 552 [58] Yona, A. H., Manor, Y. S., Herbst, R. H., Romano, G. H., Mitchell, A., Kupiec, M., Pilpel, Y.
and Dahan, O. 2012, ‘Chromosomal duplication is a transient evolutionary solution to stress.’,
Proceedings of the National Academy of Sciences **109**(51), 21010–5.
- 554 [59] Zhu, J., Pavelka, N., Bradford, W. D., Rancati, G. and Li, R. 2012, ‘Karyotypic determinants of
chromosome instability in aneuploid budding yeast’, *PLoS Genetics* **8**(5).

- 556 [60] Zhu, J., Tsai, H.-J., Gordon, M. R. and Li, R. 2018, ‘Cellular stress associated with aneuploidy’,
556 *Dev. Cell* **44**(4), 420–431.
- 558 [61] Zhu, Y. O., Sherlock, G. and Petrov, D. A. 2016, ‘Whole genome analysis of 132 clinical *Sac-*
558 *charomyces cerevisiae* strains reveals extensive ploidy variation’, *G3 Genes, Genomes, Genetics*
560 **6**(8), 2421–2434.
- 562 [62] Zhu, Y. O., Siegal, M. L., Hall, D. W. and Petrov, D. A. 2014, ‘Precise estimates of mutation rate
562 and spectrum in yeast’, *Proceedings of the National Academy of Sciences* **111**(22), E2310–E2318.

Supplementary Material

564 Supplementary Analysis

Sensitivity analysis. Changing a single parameter while keeping the rest fixed at the MAP estimate produces a worse fit to the data (Figure S6). Furthermore, we fitted models with a mutation rate fixed at $\mu = 10^{-5}$, 10^{-6} and 10^{-7} . We inferred similar parameters estimates for the model with $\mu = 10^{-6}$ compared to the model with a free μ parameter, in which the inferred mutation rate is $\mu \approx 3 \cdot 10^{-6}$. Inference assuming $\mu = 10^{-5}$ or $\mu = 10^{-7}$ produced similar estimates except that the estimated aneuploidy rate, δ , was higher, and assuming $\mu = 10^{-7}$, the estimated fitness of $2n+1$ was lower (Figure S7).

572 **Extended informative prior distribution.** In an extended informative prior distribution, we used additional growth curves of $2n^*$ (*refined* strain from Yona et al.⁵⁸) and $2n+1$ in 39 °C to estimate w_{2n^*}/w_{2n+1} (Figure S3L). The same distribution was used for w_{2n^*}/w_{2n+1*} . Thus, our main informative prior uses a single prior distribution for fitness values of $2n+1$, $2n+1^*$, and $2n^*$, whereas the extended informative prior uses one distribution for $2n+1$, and another distribution for both $2n+1^*$ and $2n^*$.

578 We estimated the parameters under this extended informative prior. Inference took much longer to run but the posterior distribution seemed to converge, as it did not change much in the final 580 iterations. The posterior predictive plot shows that inference with this extended prior produces a posterior distribution that fails to explain the empirical observations (pink in Figure 4). However, 582 the inferred posterior distribution is considerably narrower (compare Figures 3 and S8) and therefore parameter estimates are less variable. The estimated mutation rate was much lower compared to 584 the main informative prior, with $\mu = 2.474 \cdot 10^{-9}$ [$2.423 \cdot 10^{-9} - 2.612 \cdot 10^{-9}$]. Other parameter estimates are: $\delta = 2.705 \cdot 10^{-3}$ [$2.094 \cdot 10^{-3} - 3.094 \cdot 10^{-3}$], $w_{2n+1} = 1.022$ [$1.021 - 1.024$], 586 $w_{2n+1*} = 1.052$ [$1.05 - 1.054$], $w_{2n^*} = 1.053$ [$1.051 - 1.055$], the latter two being much higher compare to the main informative prior. Notably, the mode of the posterior ratio $w_{2n^*}/w_{2n+1} = 1.0009$ 588 is much lower than the mode of the prior ratio of 1.033 (Figure S3H) and closer to the ratio of 1 that we assume in the main informative prior. Together with the posterior predictive results, we conclude 590 that the main informative prior is preferable over the extended informative prior.

Model with transitions to less-fit genotypes We also estimated the parameters of a version of the

592 model that includes transitions (mutation, chromosome loss and gain) to less-fit genotypes (e.g., $2n^*$ to $2n+1^*$),

$$\begin{aligned} f_{2n}^m &= (1 - \delta - \mu)f_{2n}^s + \delta f_{2n+1}^s + \mu f_{2n+1}^s, \\ f_{2n+1}^m &= \delta f_{2n}^s + (1 - \delta - \mu)f_{2n+1}^s + \mu f_{2n+1}^s, \\ f_{2n+1}^s &= \mu f_{2n+1}^s + (1 - \delta - \mu)f_{2n+1}^s + \delta f_{2n}^s, \\ f_{2n}^s &= \mu f_{2n}^s + \delta f_{2n+1}^s + (1 - \delta - \mu)f_{2n}^s. \end{aligned} \tag{7}$$

The inferred values are slightly different. The estimated mutation rate, $\mu = 1.036 \cdot 10^{-7}$ [8.01 ·

596 $10^{-8} - 1.339 \cdot 10^{-7}$], corresponds to a mutation target size of $\sim 300 - 500$, assuming the mutation
rate per base pair is roughly $2 \cdot 10^{-10}$ (ref.⁶²) or $3.3 \cdot 10^{-10}$ (ref.²⁷). The estimated aneuploidy

598 rate, $\delta = 2.358 \cdot 10^{-4}$ [$1.766 \cdot 10^{-4} - 2.837 \cdot 10^{-4}$] is 5-35-fold higher than in previous studies:
for chromosome III in diploid *S. cerevisiae*, Zhu et al.⁶² estimated $6.7 \cdot 10^{-6}$ chromosome gain

600 events per generation, and Kumaran et al.²⁶ estimate $3.0 - 4.3 \cdot 10^{-5}$ chromosome loss events per
generation (95% confidence interval). The estimated fitness values are $w_{2n+1} = 1.024$ [1.023 – 1.025],

602 $w_{2n+1}^* = 1.025$ [1.024 – 1.026], $w_{2n} = 1.032$ [1.031 – 1.033], all relative to the fitness of $2n$, which
is set to $w_{2n} = 1$. Thus, we can infer that the cost of trisomy is $c = w_{2n} - w_{2n+1}^* = 0.007$ (or 0.7%)

604 and the benefit of trisomy is $w_{2n+1} - 1 - c = 0.017$ (1.7%), whereas the benefit of beneficial mutation
is $w_{2n} - 1 = 0.032$ (3.2%).

606 We simulated genotype frequency dynamics using parameter samples from the posterior distribution,
and computed the posterior distribution of F_A . The mean F_A in this case is just 0.0189 [0.0004 - 0.1214
608 95% CI], lower than without the transitions to less-fit genotypes. Here, F_A is the sum of frequencies
of both $2n_A^*$ and $2n + 1_A^*$, which reaches a frequency of 0.0007. Out of 100,000 posterior samples,
610 none had F_A above 0.05 (i.e., 5% of the population).

Supplementary Figures & Tables

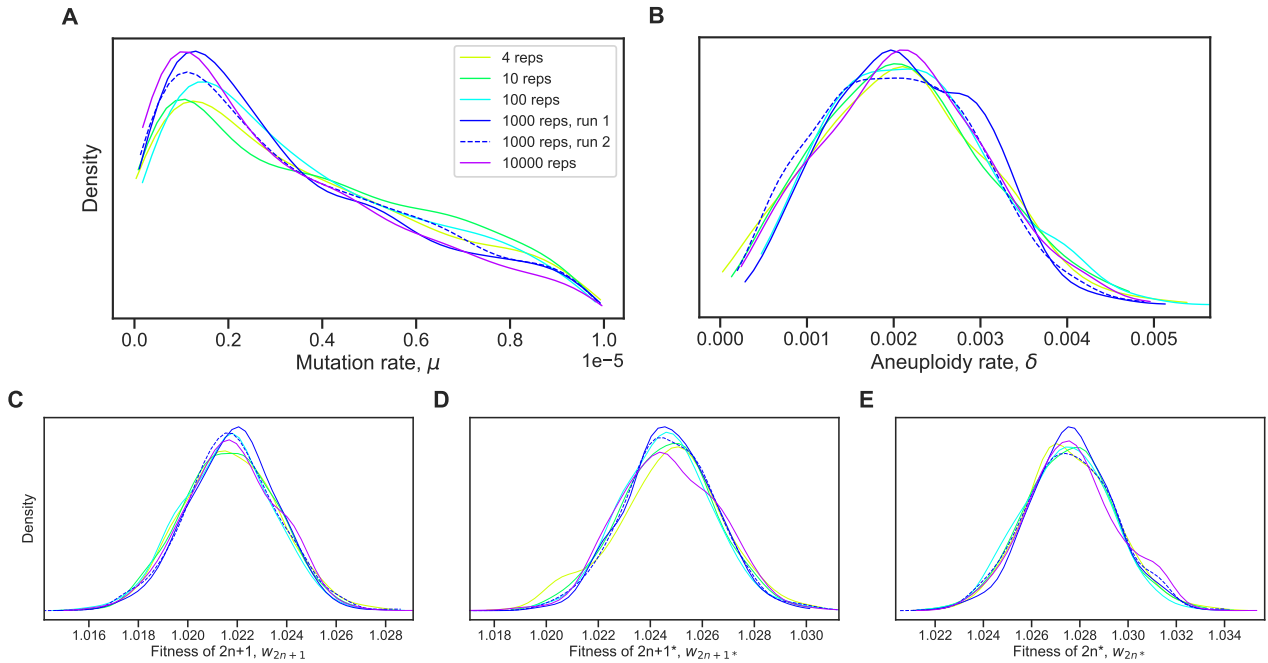


Figure S1: Posterior distribution validation. The posterior distribution of model parameters is roughly the same regardless of the number of simulations (4-10,000 replicates) used to approximate the likelihood (eq. (4)).

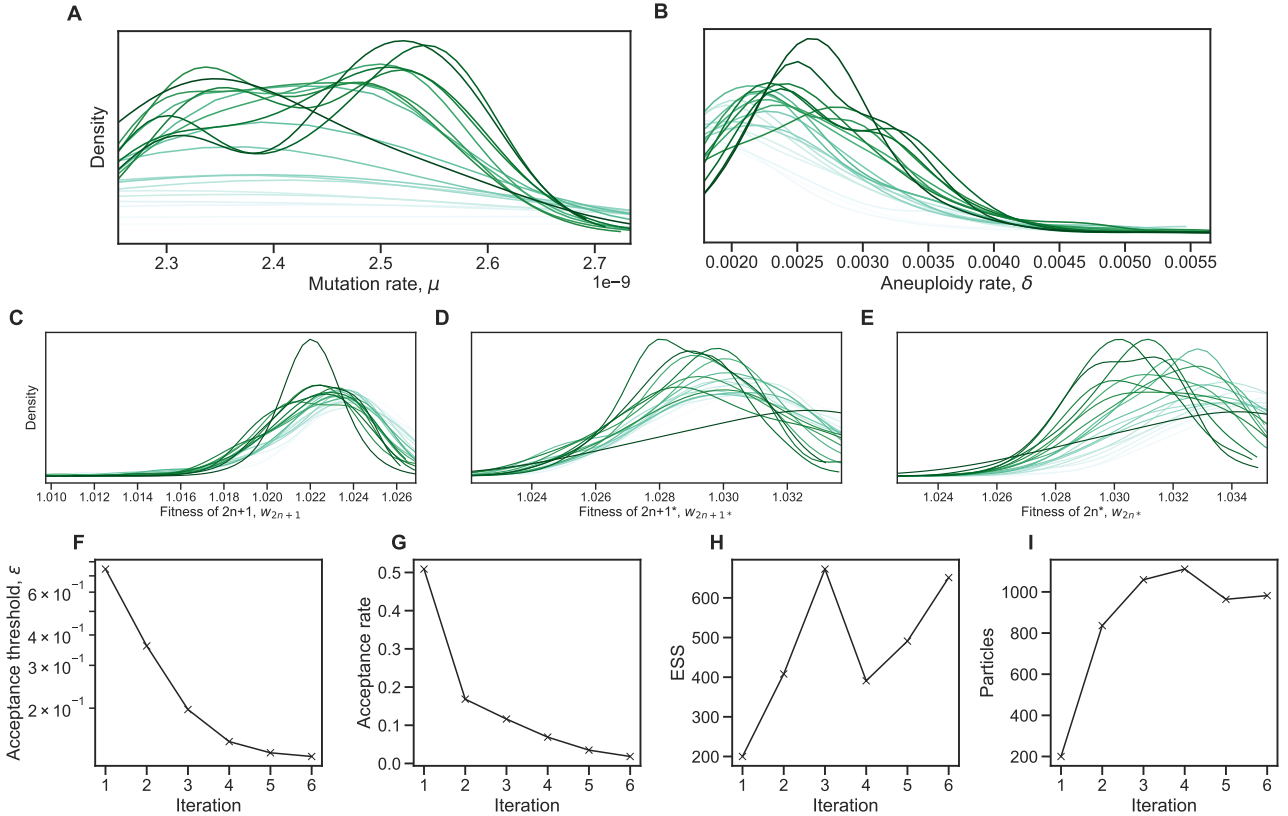


Figure S2: Inference convergence. The ABC-SMC algorithm was used to infer the model parameters. **(A-E)** The approximate posterior distributions of model parameters at each iteration of the ABC-SMC algorithm demonstrates convergence, as the posterior did not significantly change after the first iteration, $t = 1$. **(F-I)** ABC-SMC measures of convergence. After iteration number 6, the acceptance threshold was $\epsilon = 0.13$ (i.e., $\mathcal{L} = 0.87$, eq. (4)), the acceptance rate was 0.018, the number of particles was 982, and the effective sample size ESS=651.

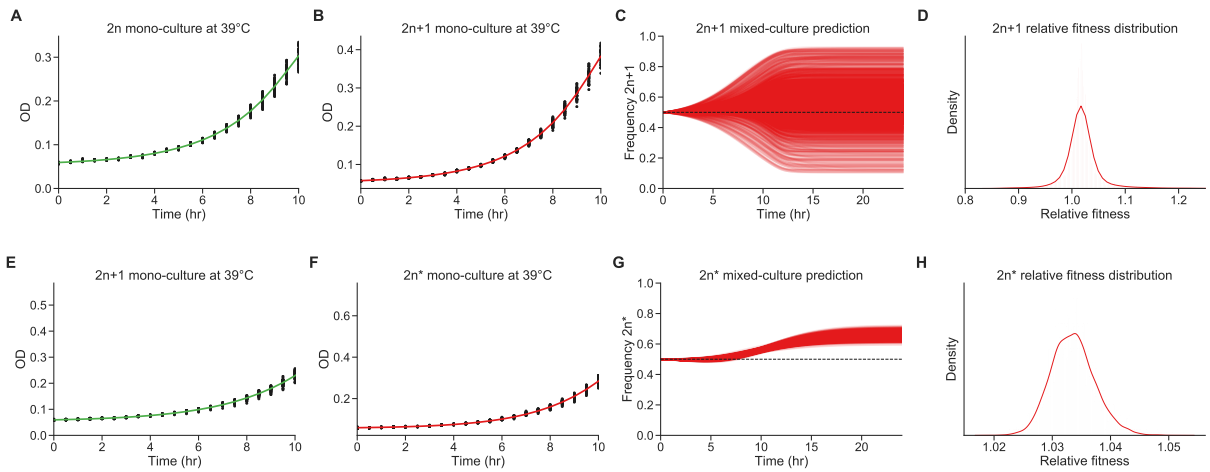


Figure S3: Fitness estimation from growth curves. **(A-D)** Fitness estimation from growth curves of $2n$ and $2n+1$ at 39°C . $w_{2n+1}/w_{2n}=1.024$ (95% CI: 0.959 - 1.115). **Curveball (E-H)** Fitness estimation from growth curves of $2n+1$ and $2n^*$ at 39°C . $w_{2n^*}/w_{2n+1}=1.033$ (95% CI: 1.027 - 1.041). Growth curves previously described in Yona et al.⁵⁸, Figs. 3C, 4A, and S2. Fitness estimated from growth curves using Curveball, a method for predicting results of competition experiments from growth curve data³⁴ curveball.yoavram.com. See *Models and Methods, Prior distributions* for more details. **(A,B;E,F)** Mono-culture growth curve data (markers) and best-fit growth models (lines). **(C,G)** The mixed-culture prediction for the strains from A,B and E,F respectively, 6,375 generated curves. **(D,H)** The relative fitness distribution for $2n+1$ relative to $2n$ (panel D) and $2n^*$ relative to $2n+1$ (panel H). Figures generated by Curveball.

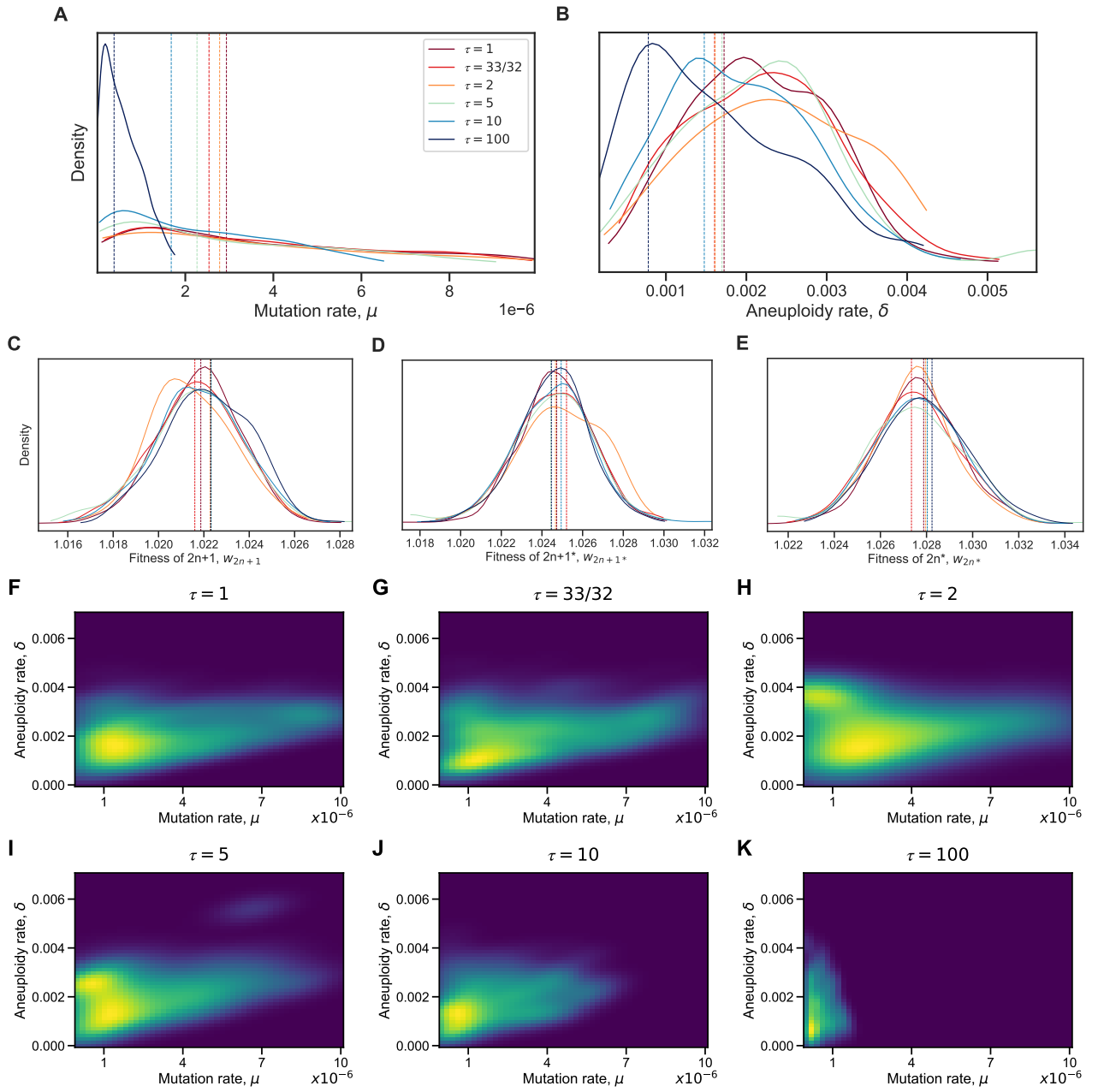


Figure S4: Model with elevated mutation rate in aneuploid cells. (A-E) The inferred posterior distributions for models with different values of τ , the fold-increase in mutation rate in aneuploid cells ($2n+1$ and $2n+1^*$). Vertical dashed lines represent the MAP (maximum a posteriori) of each distribution. When the increase in mutation rate is high, $\tau = 10$ and $\tau = 100$, the inferred mutation (A) and aneuploidy (B) rates tend to be lower. (F-K) The inferred joint posterior distribution of mutation rate (μ) and aneuploidy rate (δ) with different τ values (dark purple and bright yellow for low and high density, respectively).

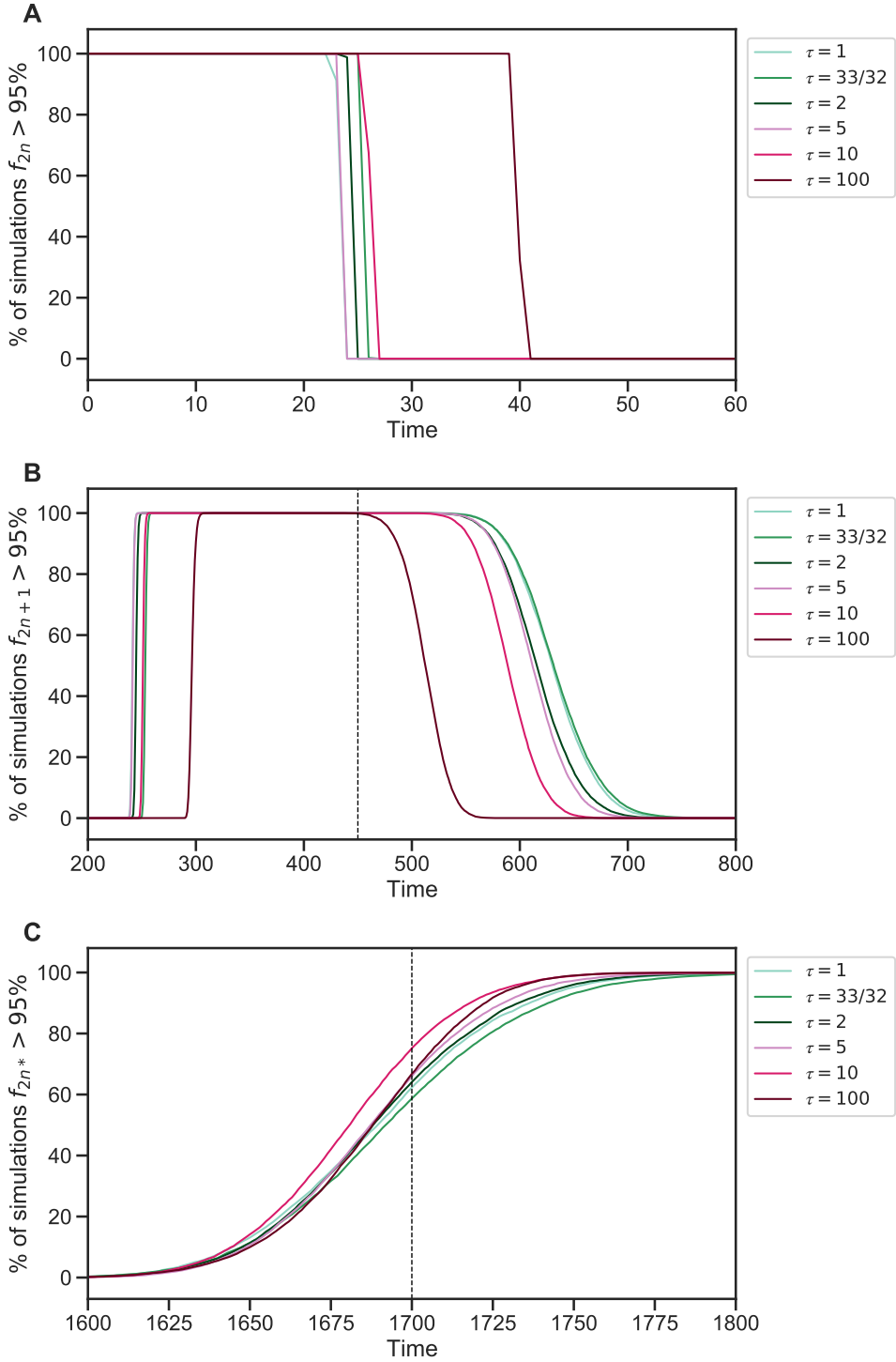


Figure S5: Genotype fixations for models with increased genetic instability. We estimated the parameters for different models, each assuming a different value of τ , the fold-increase in mutation rate in aneuploid cells. We then generated 10,000 simulations using the MAP estimate of each model and evaluated the fraction of simulations in which the frequency of genotype $2n$ (**A**), $2n+1$ (**B**), and $2n^*$ (**C**) is above 95% (y-axis) at each generation (x-axis). Note that $2n+1^*$ did not fix. We can see that $\tau = 100$ can be distinguished if the waiting time for $f_{2n} < 95\%$ is known (panel A) or if the waiting time for $f_{2n+1} > 95\%$ or $f_{2n+1} < 95\%$ is known (panel B). It is harder to distinguish between $1 \leq \tau \leq 10$.

Table S1: Mutant alleles in population $H2$.

Mutant alleles identified in the ancestor (generation 0), aneuploid (generation 450), and evolved (generation 2,350) of population $H2$. See supplementary file.

Table S2: Mutant alleles in population $H4$.

Mutant alleles identified in the ancestor (generation 0), aneuploid (generation 450), and evolved (generation 1,700) of population $H4$. See supplementary file.

Table S3: WAIC values for different τ values.

Model	WAIC
$\tau = 1$	-9
$\tau = 33/32$	-9
$\tau = 2$	-8
$\tau = 5$	-12
$\tau = 10$	-9
$\tau = 100$	-12

WAIC defined in eq. (6).

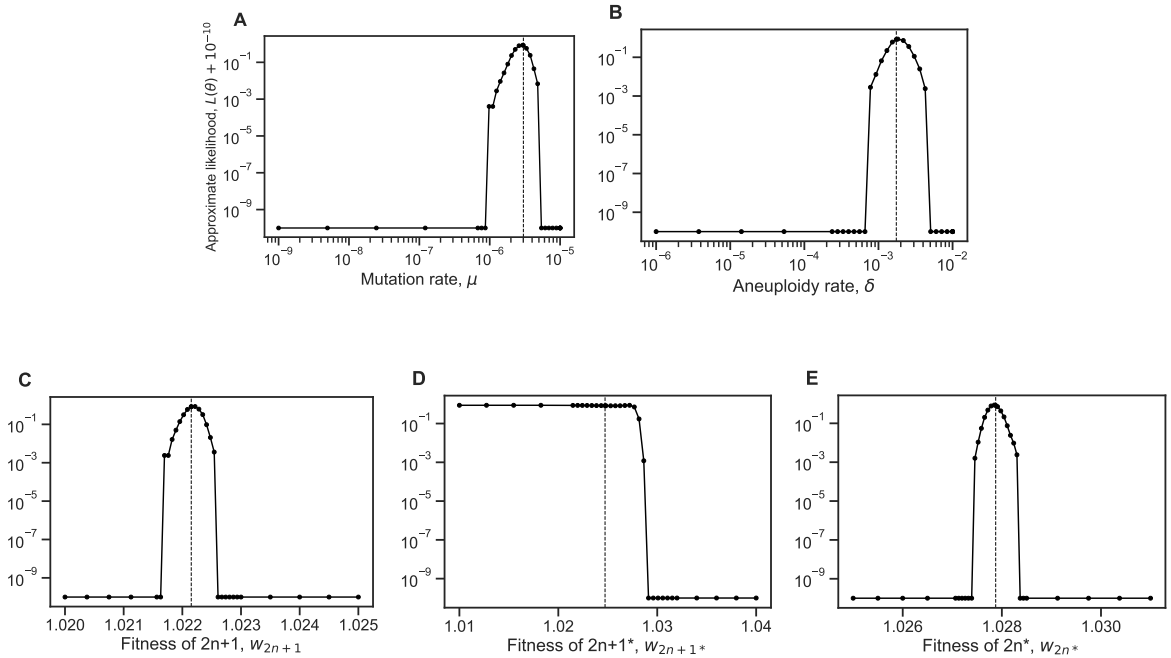


Figure S6: Likelihood profiles. Sensitivity of the model approximate likelihood, $\mathcal{L}(\theta)$, to changing a single parameter while the other parameters remain fixed at their MAP estimates. Dashed vertical line represents the MAP value. The prior distributions for the mutation rate and aneuploidy rate are $\mu \sim U(10^{-9}, 10^{-5})$ and $\delta \sim U(10^{-6}, 10^{-2})$, respectively.

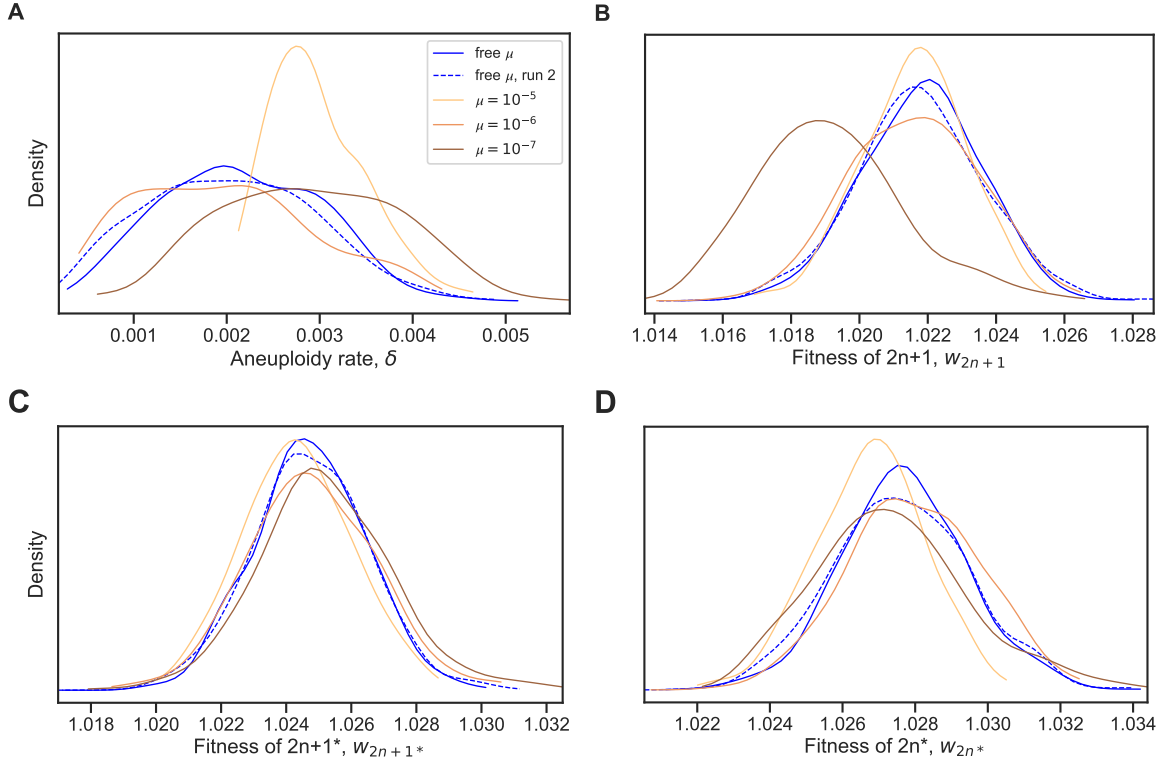


Figure S7: Model with fixed mutation rate. (A-D) The inferred posterior distributions for models with free and fixed mutation rate, μ . The MAP (maximum a posteriori) and 50% HDI (highest density interval) for each model are: **free μ , run 1:** $\delta = 1.720 \cdot 10^{-3}$ [$1.470 \cdot 10^{-3} - 2.786 \cdot 10^{-3}$], $w_{2n+1} = 1.022$ [1.021 – 1.023], $w_{2n+1^*} = 1.025$ [1.024 – 1.026], $w_{2n^*} = 1.028$ [1.026 – 1.029]; **free μ , run 2:** $\delta = 2.129 \cdot 10^{-3}$ [$1.334 \cdot 10^{-3} - 2.695 \cdot 10^{-3}$], $w_{2n+1} = 1.022$ [1.02 – 1.023], $w_{2n+1^*} = 1.025$ [1.023 – 1.026], $w_{2n^*} = 1.028$ [1.026 – 1.029]; **$\mu = 10^{-5}$:** $\delta = 2.903 \cdot 10^{-3}$ [$2.399 \cdot 10^{-3} - 3.156 \cdot 10^{-3}$], $w_{2n+1} = 1.022$ [1.021 – 1.023], $w_{2n+1^*} = 1.024$ [1.023 – 1.025], $w_{2n^*} = 1.027$ [1.026 – 1.028]; **$\mu = 10^{-6}$:** $\delta = 1.917 \cdot 10^{-3}$ [$9.624 \cdot 10^{-4} - 2.447 \cdot 10^{-3}$], $w_{2n+1} = 1.022$ [1.02 – 1.023], $w_{2n+1^*} = 1.025$ [1.023 – 1.026], $w_{2n^*} = 1.028$ [1.027 – 1.029]; **$\mu = 10^{-7}$:** $\delta = 2.901 \cdot 10^{-3}$ [$2.139 \cdot 10^{-3} - 3.671 \cdot 10^{-3}$], $w_{2n+1} = 1.019$ [1.017 – 1.02], $w_{2n+1^*} = 1.025$ [1.024 – 1.026], $w_{2n^*} = 1.027$ [1.026 – 1.029].

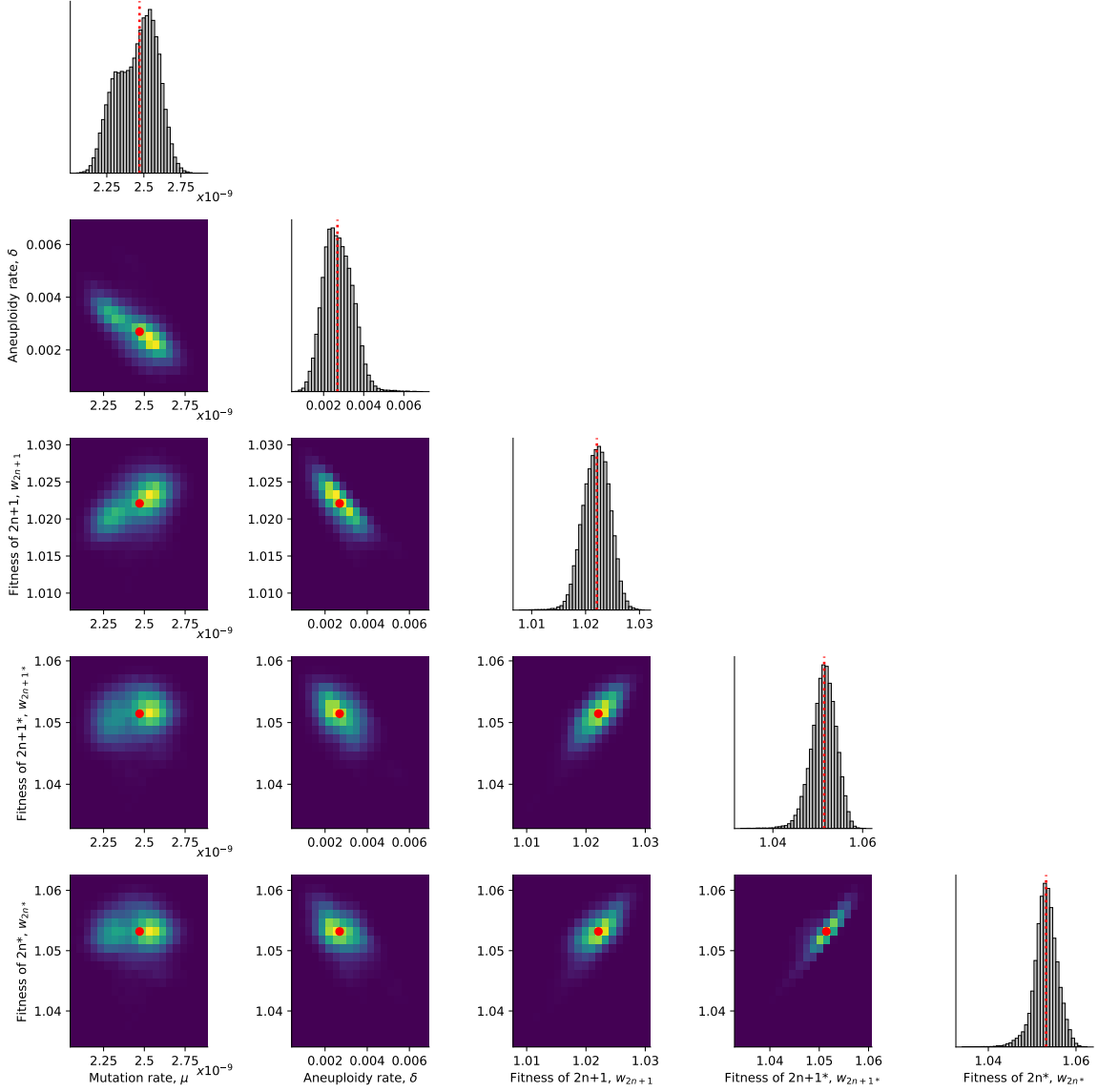


Figure S8: Posterior distribution of parameters inferred with the extended prior distribution. On the diagonal, the inferred posterior distribution of each model parameter. Below the diagonal, the inferred joint posterior distribution of pairs of model parameters (dark purple and bright yellow for low and high density, respectively). Red markers and orange lines for the joint MAP estimate (which may differ from the marginal MAP, as the marginal distribution integrates over all other parameters).

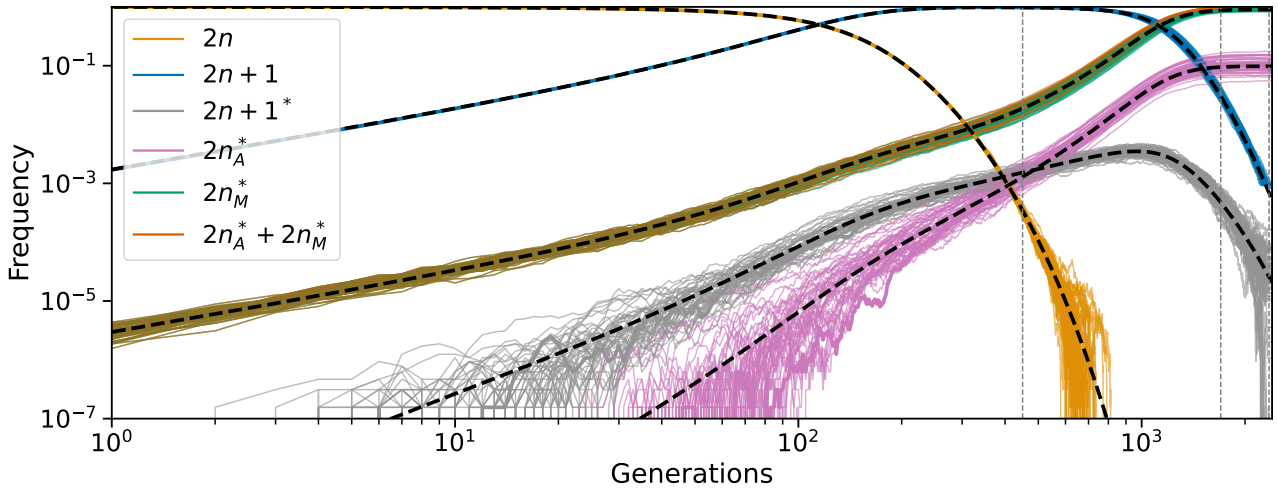


Figure S9: Posterior predicted genotype frequencies in log-log scale. Frequency dynamics of the different genotypes with MAP parameter estimates, same as Figure 5A, but in log-log scale. Black dashed curves for a deterministic model without genetic drift. Clearly, appearance of $2n+1$ and $2n_M^*$ is deterministic. Appearance of $2n+1^*$, and therefore $2n_A^*$, is stochastic, however, the frequency dynamics are deterministic above a frequency of roughly 0.001. Note that the $2n_M^*$ and the $2n_A^* + 2n_M^*$ lines are overlapping for much of their trajectories.

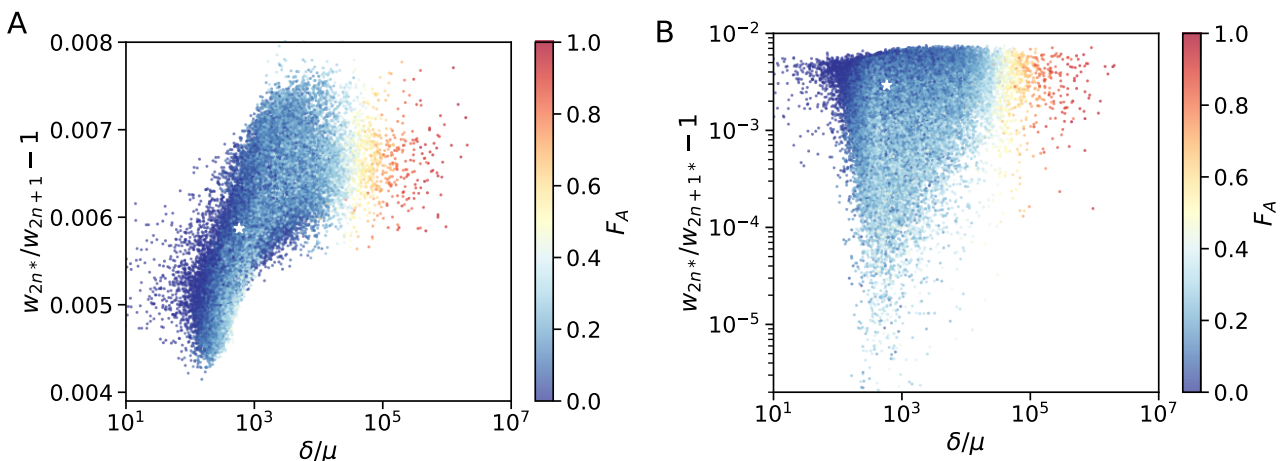


Figure S10: Posterior distribution of F_A . (A,B) F_A values (color coded) as in Figure 5 for different parameter choices on the x- and y-axes. White star denotes the MAP estimate.